

**Response to Reviewer Comments****Date: 20 September 2017****By R. Reese, T. Albrecht, M. Mengel, X. Asay-Davis and R. Winkelmann**

Journal: TC

Title: Antarctic sub-shelf melt rates via PICO

Author(s): R. Reese, T. Albrecht, M. Mengel, X. Asay-Davis and R. Winkelmann

MS No.: tc-2017-70

MS Type: Research article

First of all, we would like to thank the editor Eric Larour, the reviewer Frank Pattyn and the second, anonymous reviewer for their helpful and excellent comments and their efforts to create the detailed reviews! In our revision of the manuscript we addressed the main issues:

1. We rewrote the discussion and conclusion.
2. We changed the model to solve the governing equations per ice shelf (instead of per basin) and updated all figures and tables correspondingly.
3. We performed a forward simulation to show the capabilities of the model in combination with PISM.
4. We added a comparison with observed melt rate patterns for Filchner-Ronne and Ross ice shelves.

We provide detailed answers to all comments below. The reviewer's comments are given in black and the authors comments in blue. The changes made to the main document can be found at the end (created with latexdiff). Page and line numbers given below relate to this document.

**Referee 1: F. Pattyn**

Received and published: 24 July 2017

Interactive comment on The Cryosphere Discuss., <https://doi.org/10.5194/tc-2017-70>, 2017**General comments**

This is a great paper that fills in the gap that is currently existing in linking large scale ocean to ice-sheet models. At this time, it is probably the best alternative to fully coupled ice-shelf - ocean cavity circulation in order to determine basal melt rates underneath ice shelves. The method is based on the Olbers and Hellmer box model (OH10), but extended to two plan-view dimensions. While it encompasses a series of approximation to this simple model, it is superior to current parametrizations used in large-scale ice-sheet modelling relating melt rates to ice draft. The paper is well written and gives sufficient details on how the model is derived from OH10 and implemented numerically.

The basic premise of the PICO ocean-coupler (if I may call it so) is that circulation in ice shelf cavities is based on vertical overturning. Parameters are therefore chosen in such a way that overturning is applied to all sub-shelf cavities around Antarctica, leading to sub-shelf melting close to the grounding line and accretion (if conditions apply) away from it. Results of the model applied to present-day Antarctic ice shelves gives sub-shelf melt rates close in agreement with observed values. A brief sensitivity analysis demonstrates the effect of ocean temperatures on sub-shelf melt rates.

While the model is definitely interesting for use as an ocean coupler (in absence of fully-coupled solutions), some care should be taken in its future use: it is based on stable vertical stratification, it only considers overturning circulation under ice shelves, it neglects Coriolis effects, and it relates ocean temperature (not circulation or intrusion of CDW underneath ice shelves) to sub-shelf melt. However, major advantages are that it considers the physics of the overturning circulation and that ice shelf size (given by the number of sub-shelf boxes) and distance to grounding line and ice shelf front matters.

We would like to thank Frank Pattyn very much for his enthusiastic evaluation of our manuscript and appreciate his helpful comments for improving our study.

I have only two major comments on the paper:

1. Why using basins and not individual ice shelves to link to mean values of  $T_0$  and  $S_0$  ? It seems to me that ocean circulation (and temperature/salinity) is related to individual ice shelves and not to drainage basins, which are governed by inland ice flow. Furthermore, during prognostic simulations, these drainage boundaries may change over time, making the initial setup invalid. By treating individual ice shelves, it would also give greater detail in the coupling with ocean-model results. Furthermore, it is not complicated to implement this in a dynamical fashion.

Thanks for bringing this important point! We changed the model as suggested: we now identify single ice shelves and solve the box model equations individually for each ice shelf and not basin-wide as done before. We updated all figures and tables and changed the text to be consistent with the model improvement, e.g. in Sect. 2.3 on page 6 of the latex-diff manuscript attached below. The effect of our update is negligible for the melt rates of large ice-shelves; smaller ice shelves show slightly higher melt rates, compare Figure 1 below.

The input of PICO - which itself is a simple model - should predominantly represent the large-scale characteristics of the ocean surrounding the ice shelf. Neglecting ocean dynamics, we here approximate water masses from “source” regions upstream of the ice shelf cavities by averaging ocean properties on the depth of the continental shelf within a basin (shown in Fig. 2 of the main manuscript). These 19 regions capture the large-scale characteristics of the water masses surrounding the Antarctic continent (compare

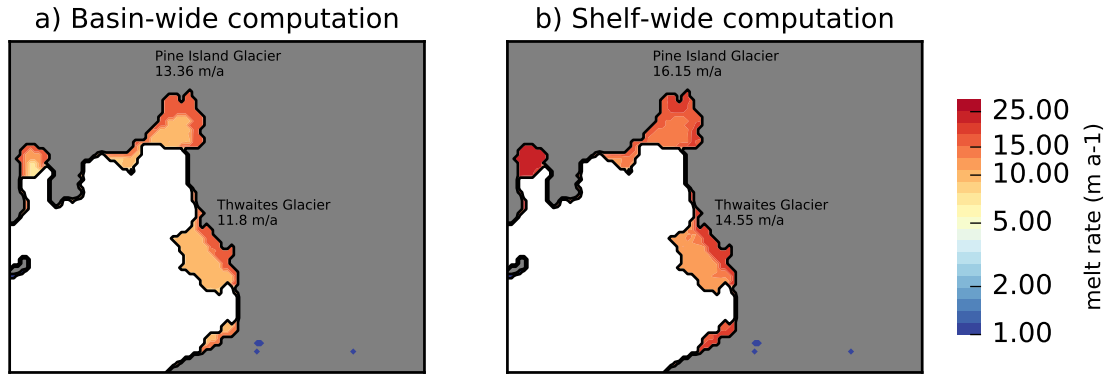


**Figure 1:** Comparison of sub-shelf melt rates underneath ice shelves in the Amundsen Sea region with the previous method (a) and the updated method that solves the box model per ice shelf (b).

Fig. 1 in Schmidtke et al. (2014)). We now link ocean input in box  $B_0$  for each ice shelf individually such that the ocean input adjusts dynamically when an ice shelf evolves across basin boundaries: The temperature and salinity values of all basins that the ice shelf belongs to are averaged, weighted by the fractional area of the shelf in the respective basin. We changed the description of PICO input in the main document accordingly, e.g., in Sect. 3, page 9, line 1ff in the latex-diff document attached.

2. While details on the implementation in PISM are given, the presented material doesn't go further than applying it to the BEDMAP2 geometry (at a given spatial resolution). Basically, the link with PISM is non-existent. It would therefore be appropriate to see how the model behaves when really applied to PISM, i.e., for an initial state (for instance spinup) close to the present day, where ice shelves are actually evolving. The only experiments shown are diagnostic, but a prognostic run would really demonstrate the capacity of the PICO coupler. Furthermore, a short run forward in time would reveal how sub-shelf conditions adapt to changing grounding-line position.

This is indeed a good point. We now provide a forward simulation based on an equilibrium state of the Antarctic Ice Sheet with a video in the Supplementary Material and discuss the adaptation of PICO to grounding line movement in the newly added Section 3.3.

Starting from equilibrium conditions for Antarctica, ocean temperatures increase linearly over 50 years until an ocean-wide warming of  $1^\circ\text{C}$  is reached and are held constant from then on. The movie shows the temporal evolution of the ocean temperature input and the sub-shelf melt rates for the ice shelf adjacent to Pine Island Glacier as well as the Filchner-Ronne Ice Shelf. The melt rates in both ice shelves increase, especially in the first boxes (spatial distribution for FRIS in the upper right panel and for PIG in the lower right panel). Subsequent ice-shelf thinning reduces the buttressing and the grounding lines retreat with the ocean boxes and melt rates adjusting accordingly.

**Detailed comments**

- P2, L1: A reference to Thoma et al (2008) “Modelling Circumpolar Deep Water intrusions on the Amundsen Sea continental shelf, Antarctica - GRL” would also be in place.

Done.

- P2, footnote: <http://www...>

Done.

- P5, L20: form stress

Done.

- P5, Eq (4): I guess there is an error in this equation, since the value of  $\rho$  will be a fractional value and not a local density. In fact, the original equation from OH10 reads

$$\rho = \rho_*(1 - \alpha(T - T_*) + \beta(S - S_*))$$

where  $T_* = 0\text{C}$  and  $S_* = 34\text{ PSU}$ . In combination with Eq (3), this then leads automatically to Eq (A9), where these two \*-values are cancelled out.

Thanks for pointing this out, this is absolutely true. We corrected the formula.

- P6, L3: Neglecting heat flux into the ice, ...

Done.

- P6, L19: see major remark: why not using ice shelves instead of basins?

Good point! We changed the code and the text here accordingly, see Sect. 2.3.

- P6; 2.3: What happens if the shelf is really thin or absent? Is the box model still applied for these contacts with the ocean?

If the ice-shelf is really thin, the model is still applied. In this case, melt rates would be low or even negative (representing accretion), depending on the input oceanic temperatures.

The model is not applied in the absence of an ice shelf, i.e., melting along vertical ice cliffs - as for example at the termini of some Greenland outlet fjords - is not modeled by PICO. We added this to the main text, see page 7, line 18 of the latex-diff attached.

- P7, 2.4: This section is irrelevant as long as the behaviour in PISM is not shown. I would therefore like to see such a simulation with the coupled system that evaluates the coupler for ice-sheet modelling beyond the diagnostic case. It would also be useful to see how it behaves when the grounding line retreats.

Thanks for bringing this to our attention. To demonstrate the behaviour of the coupled system, we made a forward run with PICO, as described in the newly added Sect. 3.3. The adjustment of the melt rates to grounding line migration can be seen in our movie (added to the Supplementary Information) with a detailed explanation in the answer to your second major comment.

- P8, L4: Even when the average of grid cells of the adjacent box is used to connect with the next box, a sharp transition (maybe less sharp) exists, as can be seen from Fig. 5. I agree that the box model can be applied locally to the shelf geometry through local variation of the ice pressure  $p$  that changes the local temperatures and salinities. However, the boundary condition to a box is given by the conditions of the adjacent box, not the conditions of a series of elements that are closest (physically this makes no sense). So, why not using just the adjacent box properties (which are mean values anyway) as a boundary condition to the local values with a box? Wouldn't this also make the model more conservative (see discussion on P15)?

Thanks for bringing this great suggestion. We changed the code accordingly and updated all tables and figures as well as the text (e.g. in Sect. 2.4, page 8, lines 15ff) correspondingly. This did substantially improve the deviation of incoming and outgoing heat fluxes from  $-867.19 \text{ GJ s}^{-1}$  (which is equivalent to  $< 5\%$  of the latent heat flux for melting) to  $403.63 \text{ GJ s}^{-1}$  (which is equivalent to  $< 2.5\%$  of the latent heat flux for melting). We do not achieve perfect conservation of energy here, since temperature in Box  $B_1$  is a non-linear function of pressure (see Eqn. A12): Averaging the results for all ice-model grid cells does not equal the result for one pressure value averaged over all ice shelf grid cells in Box  $B_1$  (see also discussion on page 16, lines 7ff).

- P8, 3: See remark on basins versus ice shelves.

We re-formulated this part of the text consistent with the updated model code (page 9 lines 1ff). Melt rates are now calculated for each shelf individually, see also our answer to your major comment #1.

- P11, L1-4: I would not consider criterion 3 and 4 criteria. 1 and 2 definitely are the basis of the overturning model; 3 and 4 are limits obtained from tuning (or validation with respect to two ice shelves), not criteria.

Thanks for this remark, this is absolutely correct. We renamed criteria 3 and 4 to “observational constraints” (1) and (2) in order to distinguish these from the qualitative model criteria (1) and (2), see page 12 lines 15ff and distinguish the criteria (black contour line) from the observational constraints (green contour line) in Fig. 4.

- P13, L2: See previous remark. I would't state that generally the melt rates are highest in the vicinity of the grounding line; that is an assumption made by the model and should be stated as such.

We changed the text to make this clear: “ Consistent with the model assumptions, melt rates ...”.

- P13, L5: Ice shelf thickness, hence pressure  $p$  is a factor that has a relatively large impact on melt rates. This is also the reason why highest melt rates within box 1 are found nearest to the grounding line. To me this is a more important observation.

Thanks for bringing these points to discussion! We added this observation. The text now reads:

“The melt pattern depends on the local pressure melting temperature. Thus, melt rates are highest where the shelf is thickest, *i.e.*, near the grounding lines within box  $B_1$ . Furthermore, freezing can occur for relatively thin ice in the same box in which melting occurs where the ice shelf is thicker. ”

- P15, Discussion: Some discussion on the limits of the model should be given. Coupled ocean-ice sheet/shelf models show that not always the maximum melt is reached at the grounding line (e.g., De Rydt and Gudmundsson (2016) Coupled ice shelf-ocean modelling and complex grounding line retreat from a seabed ridge, JGR) . Also, what are the consequences of considering overturning circulation for all ice shelves; the assumption of always having melt in box 1 and decreased melt/accretion towards the front, stable vertical stratification, and relating ocean temperature (not circulation or intrusion of CDW underneath ice shelves) to sub-shelf melt?

Thanks for bringing up these important points! We incorporated these into the Discussion:

#### **Location of maximum melting**

PICO’s design does not allow for capturing melt patterns on very local scales as described by De Rydt and Gudmundsson (2016). Their finding is consistent with further ocean simulations and observations which show lower melt rates near grounding lines but to our knowledge this is not yet widely accepted as a robust phenomenon, nor are the length or depth scales over which melt rates decay toward grounding lines well established in the literature. It is particularly important and an open question, if and how much ice dynamics are affected when the same melt flux is distributed over an area near the grounding line or a smaller area not quite reaching the grounding line. Here, we aim at covering the larger-scale features of basal melt, and in that sense we think that PICO does a good job at covering the melt in the region close to the grounding line (in PICO box  $B_1$ , see Tables 1 and 2 and the newly added Fig.S4 which compares PICO melt rates to observations).

We added a discussion of this limitation to the manuscript, see page 17 lines 25ff and 28ff.

#### **Overturning**

Following your suggestions, overturning is now calculated individually for each ice shelf (instead of per basin), yielding slightly higher melt rates for small ice shelves (see also the response to your major comment 1). The simplifying assumptions of PICO imply that one overturning value is determined per shelf; the local pattern of ocean currents underneath the ice shelf is not resolved in detail. We stated this in the discussion on page 17 in lines 14ff of the latex-diff document attached.

#### **Positive melt rates in box $B_1$**

Thanks for mentioning this, we made sure that we state this model assumption in discussion on page 18 in lines 1f of the latex diff manuscript. Melting in box  $B_1$  is a necessary

condition for the box model, but also for the ice pump. Observations indicate that melt rates are almost universally positive close to the grounding line and small areas of freezing near the grounding line would be averaged with larger areas of melting in box  $B_1$  of our model, see for example the observed sub-shelf melt rates in Fig. S4 with average melt rates annotated in each box.

#### **Stable vertical stratification**

Thanks for bringing this important point, we added it in the discussion on page 18 in lines 8-14: PICO builds on the findings of OH10 that the ocean column beneath the ice shelf is in general stratified when a steady state is reached. Furthermore, the overturning circulation as formulated in the box model is prevented from reaching neutral density and detaching from the ice-shelf base while flowing towards the shelf front. In this case, the spatial pattern of melting closer to the calving front of cold ice shelves is not represented well which may explain why PICO melt rates averaged over boxes located towards the calving front are negative in FRIS and Ross while this is not necessarily the case in the observations (see Tables 1 and 2 in this document).

#### **CDW and ocean dynamics**

PICO input is determined by averaging bottom temperatures and salinities over the continental shelf, this is done for 19 different basins. This means that PICO - which itself is a coarse model - will miss the nuances of how ocean currents transport and modify CDW over the regions being averaged. The procedure to determine melt rates in PICO is based on the assumption that ocean water that is present on the continental shelf can access the ice shelf cavities and reach their grounding lines. This implies for example, that barriers like sills that may prevent intrusion of warm CDW are not accounted for and might explain why PICO melting is too high for the ice shelves located along the Southern Antarctic Peninsula. Any such phenomena could be tested by varying the ocean input of PICO. We added this limitation to the discussion on page 18 in lines 15ff.

- P17, L2: This has not been shown in this paper and remains “potential”. Although I recognize the potential of it.

Thanks for pointing this out - we added the forward simulation to demonstrate PICO’s capabilities to adapt to grounding line migration.

**Anonymous referee 2**

Received and published: 4 August 2017

Interactive comment on The Cryosphere Discuss., <https://doi.org/10.5194/tc-2017-70>, 2017

The comment was uploaded in the form of a supplement:

<https://www.the-cryosphere-discuss.net/tc-2017-70/tc-2017-70-RC2-supplement.pdf>

**Summary**

This manuscript describes the Potsdam Ice-shelf Cavity mOdel (PICO), a new model of Antarctic ice shelf cavity circulation and the heat and freshwater exchange between the ocean and ice shelf. PICO simulates the two-dimensional overturning circulation within Antarctica's ice shelf cavities that is driven by the "ice-pump mechanism" described by the authors on page 3 lines 7-8 as "melting at the ice shelf base near the grounding line reduces salinity and the ambient ocean water becomes buoyant, rising along the ice shelf base towards the calving front." The model consists of a number of connected boxes. Denser waters from the continental shelf are transported unmodified to the grounding line in a single box, Box 0. The outflow of buoyant waters beneath the ice shelf occurs within a series of adjoining connected boxes (Box 1 through Box  $n$ ) that span the area between at the grounding line and the ice shelf calving front. T and S properties upper layer outflow boxes become progressively modified following ice melting and refreezing.

The key assumptions in this model are:

1. the inflow volume flux,  $q$ , is proportional to the density difference between the relatively denser deeper waters of the shelf outside the ice shelf (Box 0 or  $B_0$ ) and the relatively lighter waters near the grounding line (Box 1 or  $B_1$ ).
2. T and S on the outside the cavity do not evolve
3. ice shelf cavity circulation is steady-state
4. no diffusive exchanges of T and S in the vertical and horizontal directions
5. turbulent exchange parameters are constant (no flow rate dependence)
6. salinity at the ice-ocean boundary layer is that of the far-field
7. no conductive heat fluxes from the ocean into the ice shelf
8. no contribution of ice shelf meltwater into the volume flux through the upper layer boxes
9. the ocean equation of state is linearized
10. the prescribed inflow boundary conditions for all boxes of  $B_k$ ,  $k > 0$  is set as the mean of the ice-model grid cell boxes in  $B_{k-1}$  that are adjacent to  $B_k$ .

Each upper layer PICO grid cell maps to many ice shelf model grid cells. In each PICO box the ocean-ice heat and freshwater fluxes are calculated separately.

The two principal unknowns for the model are (1) the constant of proportionality,  $C$ , that sets the strength of the density-driven inflow and (2) the turbulent heat flux coefficient,  $\gamma T^*$ .

The authors use PICO with modern day values of  $T$  and  $S$  around the continental shelf to determine which set of  $C$  and  $\gamma T^*$  yield the best fit to modern day ice shelf melt rates. Using those parameter values for the entire domain they then calculate the melt rate response to varying ocean temperature variations by  $\pm 2$  C for Pine Island, Filchner-Ronne, and all Antarctica ice shelves. Melting in the cold Filchner-Ronne and Antarctica as a whole responds approximately quadratically with increasing  $T$ . In contrast, melting of the warm PIG increases approximately linearly. Both melt rate responses are consistent with earlier modelling results.

We would like to thank the reviewer very much for her/his effort, the helpful comments and the great evaluation!

### Major comments

I found this paper to be clear and well written. While I could not follow the reasoning for several of the model's assumptions I appreciated that the assumptions were articulated.

Thanks for this positive assessment. Based on your comments, we tried to make the assumptions of PICO clearer and added discussion on these and the scope of the model to the main document.

PICO is a simplified version of the Olbers and Hellmer 2010 model (OH10). If there is any major criticism to be made about this work it is that it was not clear to me why deriving a model that could be "analytically solved" is so important. While there is of course an argument for using the simplest useful model, I found myself wondering whether bits of the physics were being tossed out (e.g., heat conduction into the ice, neglect of contribution of meltwater into the volume transport, use of far-field salinity instead of the boundary-layer salinity one expects from the three-equation model, neglect of velocity dependence on turbulent flux parameter) just to make the system linear.

Thanks for bringing this to our attention! We added more discussion on the choices made in PICO and the overall scope of the model.

The aim of PICO is to introduce a simple model that computes physically-based sub-shelf melt rates and is hence preferred to parametrizations often used in current large-scale ice-sheet modelling studies that relate melt rates to the depth of the ice shelf base. We designed PICO in a way that it is easy to implement, avoiding iterative techniques or other non-linear solvers that might complicate the numerics. Nevertheless, we agree with the reviewer that all approximations

made need to be physically justified. We tried to do so here and also tried to improve the main text in this sense.

We base our discussion here on your nice summary of PICO's assumptions above. Some of these assumptions are PICO-specific, some stem from the OH10 model and others are generally made in ocean modelling. We discuss all these and their implications here and added this in the main text correspondingly, e.g., on page 4 in lines 7ff of the latex-diff document attached.

There may be a misunderstanding about assumption 2 ('T and S on the outside the cavity do not evolve'): The evolution of the input of  $T$  and  $S$  in PICO is possible. The model accepts time-dependent ocean forcing with an example given in the new Supplementary video which is discussed in the newly added Sect 3.3. The input  $T$  and  $S$  could also come from an evolving ocean model that includes freshwater fluxes taken from PICO.

Assumption 9 ('the ocean equation of state is linearized') is widely used in high-resolution models for ocean dynamics. Assumptions that are taken on from the OH10 model are:

1. the inflow volume flux,  $q$ , is proportional to the density difference between the relatively denser deeper waters of the shelf outside the ice shelf (Box 0 or  $B_0$ ) and the relatively lighter waters near the grounding line (Box 1 or  $B_1$ ).
5. turbulent exchange parameters are constant (no flow rate dependence)
7. no conductive heat fluxes from the ocean into the ice shelf
8. no contribution of ice shelf meltwater into the volume flux through the upper layer boxes

We revised the text to make this clearer, e.g., on page 4 lines 7ff and by sorting the discussion correspondingly, see pages 17 and 18.

Neglecting the velocity dependence of the turbulent flux parameters was inherited from the OH10 model. Holland and Jenkins (1999) estimate that including constant vertical heat advection reduces the computed melt rates by about 10% (their Fig. 7c). We hence omit this in PICO, but we agree that heat conduction would be a natural term to include in a coupled ice-ocean model and hence we envisage to do so in the next model version. We estimated the contribution of melt water to the volume flux to be small ( $< 1\%$  of the total overturning transport for the entire continent) and hence we regard its neglect as justified. PICO-specific assumptions are:

3. ice shelf cavity circulation is steady-state
4. no diffusive exchanges of  $T$  and  $S$  in the vertical and horizontal directions
6. salinity at the ice-ocean boundary layer is that of the far-field

The main assumption for PICO is that the overturning circulation in the cavity is in steady-state (3.). Since PICO's aim is to provide sub-shelf melt rates for large-scale ice sheet simulations and because of the much longer time scales of ice dynamics in comparison to ocean dynamics, we regard the assumption as justified. Using this assumption facilitates the adaptive box

adjustment in the case of grounding line migration or calving, especially since PICO transfers the box model approach into two horizontal dimensions. In the non-steady OH10 model, box extents and locations are fixed and to allow for evolving boxes, volume fluxes arising from box movement would add additional terms to the models' transport equations.

OH10 state that diffusive transport is small when their model reaches steady state, which justifies assumption 4, see also page 4 lines 8-10. We emphasize that using the far-field salinity (assumption 6) is only used for the computation of the sub-shelf melting directly. This linearisation of the melt equation was proposed for example by (McPhee, 1992) and was found to yield realistic heat fluxes (see e.g. Holland and Jenkins, 1999; MCPhee, 1999). As further discussed in the response to your comment regarding Page 6, lines 9-15, we do not apply this for the further calculation of the temperatures and salinities of the boxes, respectively (this would not be supported by the model equations, see discussion added on page 20, lines 25ff). While we plan to address this in the next model version, we hence believe the use of the 2-equations model for the calculation of melt rates is justified here.

Based on the reviewers' comments, we changed the way box-box transitions in PICO are done. Assumption 10 ('the prescribed inflow boundary conditions for all boxes of  $B_k$ ,  $k > 0$  is set as the mean of the ice-model grid cell boxes in  $B_{k-1}$  that are adjacent to  $B_k$ ') reads now

10B. the prescribed inflow boundary conditions for all boxes of  $B_k$ ,  $k > 0$  is set as the mean of the ice-model grid cell boxes in  $B_{k-1}$

The advantage and scope of the model described in this paper is that it is easy to implement and to verify. We hope that the additions to the text make the underlying reasoning of our approach transparent.

If PICO's simplifications assumptions were indeed made to yield a linear system of equations that could be directly solved for the purpose of numerical expediency (it is qualitatively described as "very fast" Page 16, Line 13) then it would have been useful for the authors to somehow demonstrate that or at least estimate the computational cost savings enjoyed in comparison to a more complex model such as OH10. At the end of the day, having a nonlinear set of equations that conserves energy and mass but must be solved iteratively might be preferable to one that doesn't conserve either.

Thanks for stating this. We changed the text to make the scope of our model design clearer, e.g., on page 17 in lines 10-15 of the latex-diff below. We agree that solving the entire system would not be much more expensive - given the time needed to solve the ice model equations (especially the SSA).

But, having these simple model equations has some advantages: We designed the model in a way that is easy to implement, such that other ice-sheet models can easily adopt a similar approach. Moreover, given the analytic solution, the numerical solution of PICO can easily be checked

manually, e.g., for an ice shelf with a constant thickness.

Furthermore, we argue that the errors introduced by the approximations and simplifications made in the model are of second order (see the answers to your comments above).

The mass loss in the model arises mainly from the assumption that the overturning is constant along the boxes, an assumption that introduces small errors and is similarly done in the OH10 model.

There seems to be a misunderstanding concerning the linearity of the system of equations. The temperature in box  $B_1$  is a non-linear function of pressure. Since we locally adjust the sub-shelf melt rates to the pressure melting point and use the box-wide temperature average as the boundary condition for the next box, PICO is not perfectly conserving. We find the resulting error to be small (less than 2.5% of the latent heat flux due to melting). Conservation of energy could be obtained by following your idea below and the original method of OH10, solving for a single sub-shelf melt rate with piecewise constant T and S properties in each box. The disadvantage of such an approach would be that the transition between the melt rates of the boxes would be much sharper. Also, any effect of the variation of the pressure melting point between elements within a box would be lost.

Finally, if ruthless simplification is the goal then the authors have could have gone one step further. In its present form the ocean inflow and outflow of PICO has no lateral dependence (no effect of Earth's rotation through the Coriolis effect). Instead of dividing the ice shelves into concentric rings and solving the equations in each ice-model grid cell within each box, the authors could have collapsed each ice shelf into just two dimensions and solved the equations not on the ice model grid but only in the box domain. The melt rates could then be imposed back onto the 3D ice shelf. The reason I mention this is that the concentric ring approach taken by PICO yields very strange patterns in ice melt rates (see annotated red arrows on my excerpt of Fig 5 below). Imposing that pattern of into the ice shelf model would almost certainly lead to an undesirable outcome in the long run.

This is a relevant point that is important to discuss. We did not follow the approach mentioned by the reviewer because this would not allow us to take the local pressure in every ice-sheet model grid cell into account. Collapsing the rings and solving per box (as done in the original OH10 model), would hence not allow for spatial patterns but yield a single melt rate per box. Imposing one melt rate for the entire box would yield much sharper transitions of the melt rates between the individual boxes. Also, there would be no local adjustment of the melt rates in areas thinner or thicker than the average depth within a box - suppressing an important negative feedback: If melting thins the ice-shelf, the local pressure melting point at the ice-shelf base increases and melting is reduced.

From the approach outlined in the paper, spatial melt rate patterns arise in the diagnostic solution discussed in the paper and based on the Bedmap2 geometry. In order to test your

concerns, we did a forward simulation with PICO over 300 years. The resulting evolution of the melt rates of the ice shelves in the Amundsen region and Filchner-Ronne Ice Shelf and the adjustment to grounding line migration is displayed in the newly added Supplementary Video S1. In this forward run, we find that the melt rate patterns do not yield the problems you stated. As you can see in the prognostic simulation, the ‘patches’ do not show on the ice-shelf sub-surface after 300 years (Figure 3 in this document). The negative pressure feedback tends to reduce them. The boxes’ borders are slightly visible in Filchner-Ronne Ice Shelf (left panel), which we suspect to be much sharper if one melt rate per box was determined.

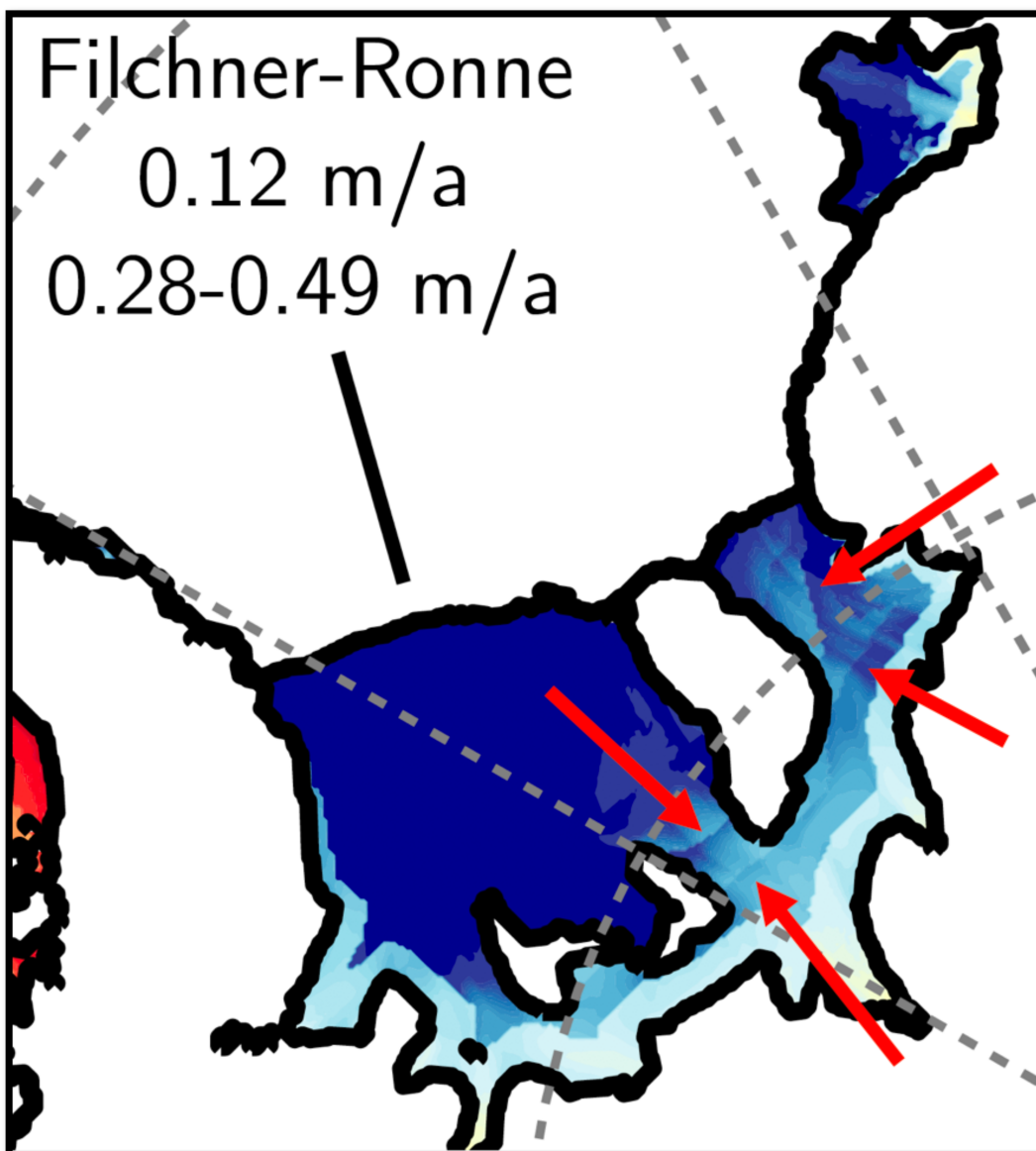
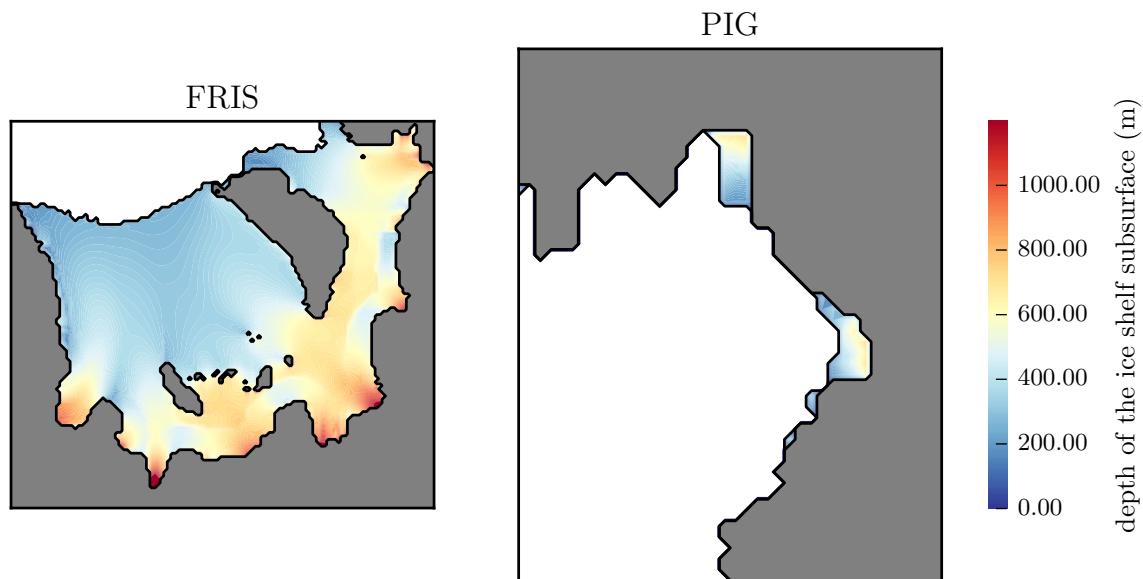


Figure 2: Inserted by reviewer 2.



**Figure 3:** Ice shelf sub-surface of Filchner Ronne Ice Shelf (left panel) and the ice shelves in the Amundsen region (right panel) after 300 years, compare also the video in the Supplementary Information.

### Minor comments

Some comparison of spatial patterns of inferred ice shelf melt rates from observations would be helpful, especially for some of the larger ice shelves, would be helpful. A zoom-in on the spatial pattern of some of the faster melting ice shelves like PIG is also advised.

This is a good point! We increased the zoom into the Amundsen region with melt rates shown for different model parameters in the Fig. S1 of the Supplementary Informations (also included in the latexdiff below). This region is also displayed in the newly added movie showing a prognostic simulation of sub-shelf melting (Supplementary Video).

We did a comparison with melt rate patterns calculated from observations described in (Moholdt et al., 2014) and obtained from (Moholdt et al., 2016) for the Filchner-Ronne and Ross ice shelves, see the newly added Fig.S4. While the general pattern of melt rates for FRIS and Ross is fairly well represented (missing, e.g., the seasonal intrusion of warm water from the calving front), the melt rates are “smoothed out” over the ice shelf: The locally observed melt rates show larger deviations from the average melting than the melt rates modelled with PICO (compare Fig. S4). Nevertheless, box-wide averages of melting show reasonable agreement from PICO and from the observations (per-box averages are given in Tables 1 and 2 with the boxes shown on top of the observational melt rates in Fig. S4). The PICO melt rates for boxes located towards the calving front are generally negative in FRIS and Ross while this is not necessarily the case in the observations - this might be explained by the fact that the overturning circulation as formulated in the box model is prevented from reaching neutral density and detaching from the ice-shelf base while flowing towards the shelf front.

**Table 1:** Melt rates from the reference simulation as displayed in Fig. S4 compared with observed values from (Moholdt et al., 2014). Melt rates are averaged over the respective box or the entire ice shelf (last row) and given in meter per year.

| FRIS  | $m_{observed}$<br>$m a^{-1}$ | $m_{PICO}$<br>$m a^{-1}$ |
|-------|------------------------------|--------------------------|
| $B_1$ | 0.42                         | 0.47                     |
| $B_2$ | 0.19                         | -0.03                    |
| $B_3$ | 0.20                         | -0.18                    |
| $B_4$ | -0.26                        | -0.13                    |
| $B_5$ | 0.53                         | -0.07                    |
| shelf | 0.26                         | 0.06                     |

**Table 2:** Melt rates from the reference simulation as displayed in Fig. S4 compared with observed values from (Moholdt et al., 2014).

| Ross  | $m_{observed}$<br>$m a^{-1}$ | $m_{PICO}$<br>$m a^{-1}$ |
|-------|------------------------------|--------------------------|
| $B_1$ | 0.05                         | 0.47                     |
| $B_2$ | -0.01                        | -0.03                    |
| $B_3$ | -0.01                        | -0.18                    |
| $B_4$ | 0.02                         | -0.13                    |
| $B_5$ | 0.28                         | -0.07                    |
| shelf | 0.08                         | 0.06                     |

Given uncertainties in the ice shelf temperatures and the ice shelf melt rates used to fit of the two free model parameters, I'd caution the authors against putting too much emphasis on the nominal values of the parameters.

We agree that this is an important point - as Fig. 4 in the main document shows, there is a whole set of parameters such that model criteria (1) and (2) are satisfied and the basin averages of the melt rates agree to some extent with observations. We changed the text accordingly, see page 19 in line 5 of the latex-diff document.

- Page 9, Line 5: “sieve criteria?” This is not a common term.

Thanks, these are simply criteria, we removed ‘sieve’.

- Page 6, lines 9-15 should be clarified.

This is an important point in the solution of the system of equations. Using the simplified melt rate formulation (called 2-equations model in (Holland and Jenkins, 1999)) was shown to yield realistic heat fluxes (McPhee, 1992) and is hence applicable in this context. For the solution of the transport equations, the underlying assumption that the boundary layer salinity  $S_{bk}$  can be replaced by the salinity of the ambient ocean water, here  $S_k$ , is however not valid: Doing so would reduce the salinity transport equation to  $S_{k-1} = S_k$

and hence the overturning circulation  $q = C(\rho_0 - \rho_1)$  would become too weak, since at the low temperatures generally present in the Southern Ocean, this circulation is mainly haline-driven. We added this discussion to the Appendix in lines 25ff on page 20 and changed the text to ‘This simplification is used only for melt rates, we nevertheless solve for the boundary layer salinity which is central to the solution of the system of equations as detailed in Appendix A’.

- Page 12, line 6: I don’t find any discussion about the procedure to determine the best-fit parameters. Perhaps you it was included in one point but it seems to be missing now. Page 12, Line 6 refers to the best fit values “found in Sect. 3.1” but 3.1 just describes the criteria and the parameter space.

Thanks for bringing to our attention that we forgot to state this! We added this explanation on page 12 lines 28ff. We determine the parameters such that the root-mean-square deviation of average melt rates for Pine Island Glacier Ice Shelf and Filchner-Ronne Ice Shelf is minimized.

- I think the conclusions section could be rewritten.

We agree and thanks you for your suggestions that we used to re-write the conclusion.

- Page 16, Line 25: your model also does not “fully reflect the circulation below ice shelves”.

Yes, we agree. We changed this to “which do not account for the circulation below ice shelves”.

- Page 16, Line 26: you didn’t validate your model to present-day ocean conditions and ice geometries, you found a set of free model parameters that yields best fit to modern day ice shelf melt rates.

We fully agree. We changed this to ‘We find a set of possible parameters for present-day ocean conditions and ice geometries which yield PICO melt rates in agreement with average melt rate observations.’

- Page 16, Line 17: I would not say that PICO “accurately” reproduces the “general” pattern of ice shelf melt with higher melting at the grounding line etc. I’d say that PICO qualitatively reproduces the general pattern of ice shelf melt with higher melting at the grounding line etc.

Thanks for bringing up this point, we changed the text accordingly on page 19 in line 7.

- Page 16, Line 30: I’d back off on the claim that you found two calibrated parameters that are “valid for the whole ice sheet”. You found a set of parameters that best fit (using a method that was not described) present-day ice shelf melt rates.

Yes, we agree. We meant that two parameters are applied for all ice shelves, and that the parameters are not adjusted for ice shelves or basins individually. We hope this is clearer with the text changed to ‘...using only two calibrated parameters applied to all ice shelves’. We added an explanation of how we determined the best-fit parameters on page 12 in lines 28ff of the latex-diff document attached.

## References

- De Rydt, J. and Gudmundsson, G. H. (2016). Coupled ice shelf-ocean modeling and complex grounding line retreat from a seabed ridge. *Journal of Geophysical Research: Earth Surface*, 121(5):865–880. 2015JF003791.
- Holland, D. M. and Jenkins, A. (1999). Modeling Thermodynamic Ice-Ocean Interactions at the Base of an Ice Shelf. *Journal of Physical Oceanography*, 29(8):1787–1800.
- McPhee, M. G. (1992). Turbulent heat flux in the upper ocean under sea ice. *Journal of Geophysical Research: Oceans*, 97(C4):5365–5379.
- McPhee, M. G. (1999). Parameterization of mixing in the ocean boundary layer. *Journal of Marine Systems*, 21(1-4):55–65.
- Moholdt, G., Padman, L., and Fricker, H. A. (2014). Basal mass budget of Ross and Filchner-Ronne ice shelves, Antarctica, derived from Lagrangian analysis of ICESat altimetry. *Journal of Geophysical Research: Earth Surface*, 119(11):2361–2380. 2014JF003171.
- Moholdt, G., Padman, L., and Fricker, H. A. (2016). Elevation change and mass budget of Ross and Filchner-Ronne ice shelves, Antarctica.
- Schmidtko, S., Heywood, K. J., Thompson, A. F., and Aoki, S. (2014). Multidecadal warming of Antarctic waters. *Science*, 346(6214):1227–1231.

# Antarctic sub-shelf melt rates via PICO

Ronja Reese<sup>1,3</sup>, Torsten Albrecht<sup>1</sup>, Matthias Mengel<sup>1</sup>, Xylar Asay-Davis<sup>1,2</sup>, and Ricarda Winkelmann<sup>1,3</sup>

<sup>1</sup> Potsdam Institute for Climate Impact Research (PIK), Member of the Leibniz Association, P.O. Box 60 12 03, D-14412 Potsdam, Germany

<sup>2</sup> Los Alamos National Laboratory, P.O. Box 1663, T-3, MS-B216, Los Alamos, NM 87545, United States

<sup>3</sup> University of Potsdam, Institute of Physics and Astronomy, Karl-Liebknecht-Str. 24-25, 14476 Potsdam, Germany

*Correspondence to:* Ricarda Winkelmann (ricarda.winkelmann@pik-potsdam.de)

**Abstract.** Ocean-induced melting below ice shelves is one of the dominant drivers for mass loss from the Antarctic Ice Sheet at present. An appropriate representation of sub-shelf melt rates is therefore essential for model simulations of marine-based ice sheet evolution. Continental-scale ice sheet models often rely on simple melt-parameterizations, in particular for long-term simulations, when fully coupled ice-ocean interaction becomes computationally too expensive. Such parameterizations can account for the influence of the local depth of the ice-shelf draft or its slope on melting. However, they do not capture the effect of ocean circulation underneath the ice-shelf. Here we present the Potsdam Ice-shelf Cavity mOdel (PICO), which simulates the vertical overturning circulation in ice-shelf cavities and thus enables the computation of sub-shelf melt rates consistent with this circulation. PICO is based on an ocean box model that coarsely resolves ice shelf cavities and uses a boundary layer melt formulation. We implement it as a module of the Parallel Ice Sheet Model (PISM) and evaluate its performance under present-day conditions of the Southern Ocean. The two-dimensional melt rate fields provided by the model reproduce the typical pattern of comparably high melting near the grounding line and lower melting or refreezing towards the calving front. PICO captures the wide range of melt rates observed for Antarctic ice shelves, with an average of about  $0.1 \text{ m a}^{-1}$  for cold sub-shelf cavities, for example underneath Ross or Ronne ice shelves, to  $\sim 16 \text{ m a}^{-1}$  for warm cavities such as in the Amundsen Sea region. This makes PICO a computationally-feasible and more physical alternative to melt parameterizations purely based on ice draft geometry.

## 1 Introduction

Dynamic ice discharge across the grounding lines into floating ice shelves is the main mass loss process of the Antarctic Ice Sheet. Surrounding most of Antarctica's coastlines, the ice shelves themselves lose mass by ocean-induced melting from below or calving of icebergs (Depoorter et al., 2013; Liu et al., 2015). Observations show that many Antarctic ice shelves are thinning at present, driven by enhanced sub-shelf melting (Pritchard et al., 2012; Paolo et al., 2015). Thinning reduces the ice shelves' buttressing potential, *i.e.*, the restraining force at the grounding line provided by the ice shelves (Thomas, 1979; Dupont and Alley, 2005; Gudmundsson et al., 2012), and can thereby accelerate upstream glacier flow. The observed acceleration of tributary glaciers is seen as the major contributor to the current mass loss in the West Antarctic Ice Sheet (Pritchard et al., 2012). In particular, the recent dynamic ice loss in the Amundsen Sea sector (MacGregor et al., 2012; Mouginot et al., 2014) is

associated with high melt rates that result from inflow of relatively warm circumpolar deep water (CDW) in the ice shelf cavities (Holland et al., 2008a; Jacobs et al., 2011; Pritchard et al., 2012; Schmidtke et al., 2014; Hellmer et al., 2017) (Holland et al., 2008a; Jaco

Also in East Antarctica, particularly at Totten glacier, as well as along the Southern Antarctic Peninsula, glacier thinning seems to be linked to CDW reaching the deep grounding lines (Greenbaum et al., 2015; Wouters et al., 2015). An appropriate representation of melt rates at the ice-ocean interface is hence crucial for simulating the dynamics of the Antarctic Ice Sheet. Melting in ice-shelf cavities can occur in different modes that depend on the ocean properties in the proximity of the ice shelf, the topography of the ocean bed and the ice-shelf subsurface (Jacobs et al., 1992). Antarctica’s ice shelf cavities can be classified into “cold” and “warm” with typical mean melt rates ranging from  $\mathcal{O}(0.1 - 1.0) \text{ m a}^{-1}$  in “cold” cavities as for the Filchner-Ronne Ice Shelf and  $\mathcal{O}(10) \text{ m a}^{-1}$  in “warm” cavities like the one adjacent to Pine Island Glacier (Joughin et al., 2012). For the “cold” cavities of the large Ross, Filchner-Ronne and Amery ice shelves, freezing to the shelf base is observed in the shallower areas near the center of the ice shelf and towards the calving front (Rignot et al., 2013; Moholdt et al., 2014).

Since the stability of the ice sheet is strongly linked to the dynamics of the buttressing ice shelves, it is essential to adequately represent their mass balance. A number of parameterizations with different levels of complexity have been developed to capture the effect of sub-shelf melting. Simplistic parameterizations that depend on the local ocean and ice-shelf properties have been applied in long-term and large-scale ice sheet simulations (Joughin et al., 2014; Martin et al., 2011; Pollard and DeConto, 2012; Favier et al., 2014). These parameterizations make melt rates piece-wise linear functions of the depth of the ice-shelf draft (Beckmann and Goosse, 2003) or of the slope of the ice-shelf base (Little et al., 2012). Other models describe the evolution of melt-water plumes forming at the ice-shelf base (Jenkins, 1991). Plumes evolve depending on the ice-shelf draft and slope, sub-glacial discharge and entrainment of ambient ocean water. This approach has been applied to models with characteristic conditions for Antarctic ice shelves (Holland et al., 2007; Payne et al., 2007) and for Greenland outlet glaciers and fjord systems (Jenkins, 2011; Carroll et al., 2015). Interactively coupled ice-ocean models that resolve both the ice flow and the water circulation below ice shelves are now becoming available (Goldberg et al., 2012; Thoma et al., 2015; Seroussi et al., 2017; De Rydt and Gudmundsson, 2016). There is a community effort to better understand effects of ice-ocean interaction in such coupled models (Asay-Davis et al., 2016). However, as ocean models have many more degrees of freedom than ice sheet models and require for much shorter time steps, coupled simulations are currently limited to short time scales (on the order of decades to centuries).

Here, we present the Potsdam Ice-shelf Cavity mOdel (PICO), which provides sub-shelf melt rates in a computationally efficient manner and resolves the basic vertical overturning circulation in ice shelf cavities driven by the ice pump (Lewis and Perkin, 1986). It is based on the earlier work of Olbers and Hellmer (2010) and is implemented as a module in the Parallel Ice Sheet Model (PISM: Bueler and Brown, 2009; Winkelmann et al., 2011)<sup>1</sup>. Ocean temperature and salinity at the depth of the bathymetry in the continental shelf region serve as input data. PICO allows for long-term simulations (on centennial to millennial time scales) and for large ensembles of simulations which makes it applicable, for example, in paleo-climate studies or as a coupling module between ice-sheet and Earth System models.

---

<sup>1</sup><http://www.pism-docs.org>

**Table 1.** PICO parameters and typical values.

| Parameter   | Symbol       | Value                 | Unit                                      |
|---|--------------|-----------------------|---|
| Salinity coefficient of freezing equation         | $a$          | $-0.0572$             | $^{\circ}\text{C PSU}^{-1}$               |
| Constant coefficient of freezing equation         | $b$          | $0.0788$              | $^{\circ}\text{C}$                        |
| Pressure coefficient of freezing equation         | $c$          | $7.77 \times 10^{-8}$ | $^{\circ}\text{C Pa}^{-1}$                |
| Thermal expansion coefficient in EOS              | $\alpha$     | $7.5 \times 10^{-5}$  | $^{\circ}\text{C}^{-1}$                   |
| Salt contraction coefficient in EOS               | $\beta$      | $7.7 \times 10^{-4}$  | $\text{PSU}^{-1}$                         |
| Reference density in EOS                          | $\rho_*$     | $1033$                | $\text{kg m}^{-3}$                        |
| Latent heat of fusion                             | $L$          | $3.34 \times 10^5$    | $\text{J kg}^{-1}$                        |
| Heat capacity of sea water                        | $c_p$        | $3,974$               | $\text{J kg}^{-1} ^{\circ}\text{C}^{-1}$  |
| Density of ice                                    | $\rho_i$     | $910$                 | $\text{kg m}^{-3}$                        |
| Density of sea water                              | $\rho_w$     | $1028$                | $\text{kg m}^{-3}$                        |
| Turbulent salinity exchange velocity              | $\gamma_S$   | $2 \times 10^{-6}$    | $\text{m s}^{-1}$                         |
| Turbulent temperature exchange velocity           | $\gamma_T$   | $5 \times 10^{-5}$    | $\text{m s}^{-1}$                         |
| Effective turbulent temperature exchange velocity | $\gamma_T^*$ | $2 \times 10^{-5}$    | $\text{m s}^{-1}$                         |
| Overturning strength                              | $C$          | $1 \times 10^6$       | $\text{m}^6 \text{s}^{-1} \text{kg}^{-1}$ |

The coefficients in the equation of state (EOS), the turbulent exchange velocities for heat and salt are taken from Olbers and Hellmer (2010). We linearized the potential freezing temperature equation with a least-squares fit with salinity values over a range of 20-40 PSU and pressure values of 0-10<sup>7</sup> Pa using Gibbs SeaWater Oceanographic Package of TEOS-10 (McDougall and Barker, 2011). All values are kept constant, except for  $\gamma_T^*$  and  $C$ , which vary between experiments. The values of these two parameters are the best-fit from Sect. 3.1.

In this paper, we give a brief overview of the cavity circulation and melt physics and describe the ocean box geometry in PICO and implementation in PISM in Sect. 2. In Section 3, we derive a valid parameter range for present-day Antarctica and compare the resulting sub-shelf melt rates to observational data. This is followed by a discussion of the applicability and limitations of the model (Sect. 4) and conclusions (Sect. 5).

## 5 2 Model description

PICO is developed from the ocean box model of Olbers and Hellmer (2010), henceforth OH10. The OH10 model is designed to capture the basic overturning circulation in ice shelf cavities which is driven by the “ice pump” mechanism: melting at the ice shelf base near the grounding line reduces salinity and the ambient ocean water becomes buoyant, rising along the ice shelf base towards the calving front. Since the ocean temperatures on the Antarctic continental shelf are generally close to the local freezing point, density variations are primarily controlled by salinity changes. Melting at the ice-shelf base hence reduces the density of ambient water masses, resulting in a haline-driven circulation. Buoyant water rising along the shelf base draws in ocean water at depth, which flows across the continental shelf towards the deep grounding lines of the ice shelves. The warmer these water masses are, the stronger is the melting-induced ice pump. The OH10 box model describes the relevant physical

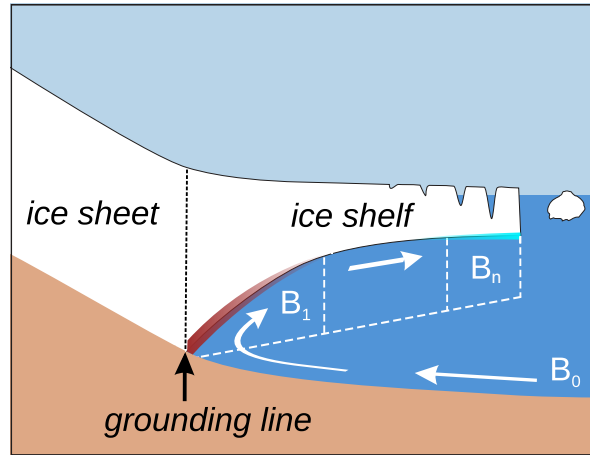


**Figure 1.** Schematic view of the PICO model. The model mimics the overturning circulation in ice shelf cavities: Ocean water from box  $B_0$  enters the ice shelf cavity at the depth of the sea floor and is advected to the grounding line box  $B_1$ . Freshwater influx from melting at the ice shelf base makes the water buoyant, causing it to rise. The cavity is divided into  $n$  boxes along the ice shelf base. Generally, the highest melt rates can be found near the grounding line, with lower melt rates or refreezing towards the calving front.

processes and captures this vertical overturning circulation by defining consecutive boxes following the flow within the ice shelf cavity.

The strength of the overturning flux  $q$  is determined from the density difference between the incoming water masses on the continental shelf and the buoyant water masses near the deep grounding lines of the ice shelf.

5 As PICO is implemented in an ice sheet model with characteristic time scales much slower than typical response times of the ocean, we assume steady-state ocean conditions and hence reduce the complexity of the governing equations of the OH10 model. Using this assumption facilitates the adaptive box adjustment to grounding line migration, especially since PICO transfers the box model approach into two horizontal dimensions. We assume stable vertical stratification, ~~which~~; OH10 found that a circulation state for an unstable vertical water column, which would imply a high (parametrized) diffusive transport  
 10 between boxes, only occurs transiently (Olbers and Hellmer, 2010, Sect. 2). This motivates neglecting the diffusive heat and salt transport between boxes<sup>2</sup> which is small under these conditions. Without diffusive transport between the boxes, some of the original ocean boxes from OH10 become passive and can be incorporated into the governing equations of the set of boxes used in PICO. We explicitly model a single open ocean box which provides the boundary conditions for the boxes adjacent to the ice shelf base following the overturning circulation, as shown in Fig. 1. In order to better resolve the complex melt  
 15 patterns, PICO adapts the number of boxes based on the evolving geometry of the ice shelf. These simplifying assumptions allow us to analytically solve the system of governing equations, which is presented in the following two sections. A detailed

<sup>2</sup>~~OH10 discuss a circulation state for an unstable vertical water column, which would imply a high (parametrized) diffusive transport between boxes. They find that this state only occurs transiently (Olbers and Hellmer, 2010, Sect. 2).~~

derivation of the analytic solutions is given in Appendix A. In Sect. 2.3, we describe how the ice-model grid relates to the ocean box geometry of PICO. The system of equations is solved locally on the ice-model grid, as described in Sect. 2.4. Table 1 summarizes the model parameters and typical values.

## 2.1 Physics of the overturning circulation in ice shelf cavities

- 5 PICO solves for the transport of heat and salt between the ocean boxes as depicted in Fig. 1. Although box  $B_0$ , which is located at depth between the ice shelf front and the edge of the continental shelf, does not extend into the shelf cavity, its properties are transported unchanged from box  $B_0$  to box  $B_1$  near the grounding line. The heat and salt balances for all boxes in contact with the ice shelf base (boxes  $B_k$  for  $k \in \{1, \dots, n\}$ ) can be written as

$$V_k \dot{T}_k = qT_{k-1} - qT_k + A_k m_k T_{bk} - A_k m_k T_k + A_k \gamma_T (T_{bk} - T_k) \quad (1)$$

$$10 \quad V_k \dot{S}_k = qS_{k-1} - qS_k + A_k m_k S_{bk} - A_k m_k S_k + A_k \gamma_S (S_{bk} - S_k). \quad (2)$$

The local application of these equations for each ice model cell is described in Sect. 2.4. Since we assume steady circulation, the terms on the left-hand side are neglected. For the box  $B_k$  with volume  $V_k$ , heat or salt content change due to advection from the adjacent box  $B_{k-1}$  with overturning flux  $q$  (first term on the right-hand side) and due to advection to the neighboring box  $B_{k+1}$  (or the open ocean for  $k = n$ ) ~~with overturning flux  $q$~~  (second term). Vertical melt flux into the box  $B_k$  across the ice-ocean interface with area  $A_k$  (third term) and out of the box (fourth term) play a minor role and are neglected in the analytic solution of the equation system employed in PICO (a detailed discussion of these terms is given in Jenkins et al., 2001). The melt rate  $m_k$  is negative if ambient water freezes to the shelf base. The last term represents heat and salt changes via turbulent, vertical diffusion across the boundary layer beneath the ice-ocean interface. The parameters  $\gamma_T$  and  $\gamma_S$  are the turbulent heat and salt exchange velocities which we assume, [following OH10](#), to be constant.

- 20 The overturning flux  $q > 0$  is assumed to be driven by the density difference between the ocean reservoir box  $B_0$  and the grounding line box  $B_1$ . This is parametrized as [in OH10](#)

$$q = C(\rho_0 - \rho_1) \quad (3)$$

where  $C$  is a constant overturning coefficient that captures effects of friction, rotation and bottom ~~formstress~~[form stress](#)<sup>2</sup>. The circulation strength in PICO is hence determined by density changes through sub-shelf melting in the grounding zone box  $B_1$ .

25 From there, water follows the ice shelf base towards the open ocean assuming the overturning flux  $q$  to be the same for all subsequent boxes. Ocean water densities are computed assuming a linear approximation of the equation of state

$$\rho = \rho_* (1 - \alpha \underline{T(T - T_*)} + \beta \underline{(S - S_*)}) \quad (4)$$

where [T\\* = 0 °C](#), [S\\* = 34 PSU](#) and  $\alpha$ ,  $\beta$  and  $\rho_*$  are constants with values given in Table 1.

<sup>2</sup>For a more detailed discussion see Olbers and Hellmer (2010, Sect. 2).

## 2.2 Melting physics

Melting physics are derived from the widely used 3-equation model (Hellmer and Olbers, 1989; Holland and Jenkins, 1999) which assumes the presence of a boundary layer below the ice-ocean interface. The temperature at this interface in box  $B_k$  is assumed to be at the in-situ freezing point  $T_{bk}$ , which is linearly approximated by

$$5 \quad T_{bk} = aS_{bk} + b - cp_k, \quad (5)$$

where  $p_k$  is the overburden pressure, here calculated as static-fluid pressure given by the weight of the ice on top. At the ice-ocean interface, the heat flux from the ambient ocean across the boundary layer due to turbulent mixing,  $Q_T = \rho_w c_p \gamma_T (T_{bk} - T_k)$ , equals the heat flux due to melting or freezing  $Q_{Tb} = -\rho_i L m_k$ . ~~We here neglect~~ Neglecting heat flux into the ice, the heat balance equation thus reads

$$10 \quad \gamma_T (T_{bk} - T_k) = -\nu \lambda m_k \quad (6)$$

where  $\nu = \rho_i / \rho_w \sim 0.89$ ,  $\lambda = L / c_p \sim 84^\circ\text{C}$ . We obtain the salt flux boundary condition as the balance between turbulent salt transfer across the boundary layer,  $Q_S = \rho_w \gamma_S (S_{bk} - S_k)$ , and reduced salinity due to melt water input,  $Q_{Sb} = -\rho_i S_{bk} m_k$ ,

$$\gamma_S (S_{bk} - S_k) = -\nu S_{bk} m_k. \quad (7)$$

To compute melt rates, we apply a simplified version of the 3-equations model (McPhee, 1992, 1999; Holland and Jenkins, 15 1999) which allows for a simple, analytic solution of the system of governing equations. It has been shown that this formulation yields realistic heat fluxes (McPhee, 1992, 1999). This simplification is used only for melt rates, ~~the 3-equations formulation is applied from then on, with details laid out~~ we nevertheless solve for the boundary layer salinity which is central to the solution of the system of equations as detailed in Appendix A. Melt rates are given by

$$m_k = -\frac{\gamma_T^*}{\nu \lambda} (aS_k + b - cp_k - T_k) \quad (8)$$

20 with ambient ocean temperature  $T_k$  and salinity  $S_k$  in box  $B_k$ . Here, we use the effective turbulent heat exchange coefficient  $\gamma_T^*$ . The relation between  $\gamma_T$  and  $\gamma_T^*$  is discussed in the Appendix A.

## 2.3 PICO ocean box geometry

PICO is implemented as a module in the three-dimensional ice sheet model PISM as described in Sect. 2.4. Since the original system of box-model equations is formulated for only one horizontal and one vertical dimension, it needed to be extended for 25 the use in the three-dimensional ice sheet model. ~~To this aim, PICO distinguishes basins, which are chosen to encompass large ice shelf embayments and areas of similar ocean conditions. The standard basins used for Antarctica are shown in Fig. 2, see Sect. 3.~~ The system of governing equations as described in the previous two sections ~~are~~ is solved for each ~~basin independently. ice shelf independently. PICO adapts the ocean boxes to the evolving ice shelves at every time step.~~

For any ~~basin shelf~~ basin shelf  $D$ , we determine the number of ocean boxes  $n_D$  ~~based on the~~ by interpolating between 1 and  $n_{\max}$  30 depending on its size and geometry ~~of the ice shelves~~ such that larger ice shelves are resolved with more boxes. The ~~number of~~

boxes is defined separately for each basin by interpolating between 1 and  $n_{\max}$  depending on the geometry of the ice shelves within that basin. The maximum number of boxes  $n_{\max}$  is a model parameter; a value of 5 is used suitable for the Antarctic setup, as discussed further in Sect 3.2. We determine the number of boxes  $n_D$  for the basin each individual ice shelf  $D$  with

$$n_D = 1 + \text{rd} \left( \sqrt{d_{\text{GL}}(D)/d_{\max}} (n_{\max} - 1) \right) \quad (9)$$

- 5 where  $\text{rd}(\cdot)$  rounds to the nearest integer. Here,  $d_{\text{GL}}(x, y)$  is the local distance to the grounding line from an ice-model grid cell with horizontal coordinates  $(x, y)$ ,  $d_{\text{GL}}(D)$  is the maximum distance within basin-ice shelf  $D$  and  $d_{\max}$  is the maximum distance to the grounding line in the entire domain. PICO adapts the ocean boxes to the evolving ice shelves at every time step within the entire computational domain.

- Knowing the maximum number of boxes  $n_D$  for a basin an ice shelf  $D$ , we next define the ocean boxes underneath the ice shelves within that basin it. The extent of boxes  $B_1, \dots, B_{n_D}$  is determined using the distance to the grounding line and the shelf front. The non-dimensional relative distance to the grounding line relative distance to the grounding line  $r$  is defined as

$$r(x, y) = d_{\text{GL}}(x, y) / (d_{\text{GL}}(x, y) + d_{\text{IF}}(x, y)) \quad (10)$$

with  $d_{\text{IF}}(x, y)$  the horizontal distance to the ice front. We assign all ice cells with horizontal coordinates  $(x, y) \in D$  to box  $B_k$  if the following condition is met

$$15 \quad 1 - \sqrt{(n_D - k + 1)/n_D} \leq r(x, y) \leq 1 - \sqrt{(n_D - k)/n_D}. \quad (11)$$

This leads to comparable areas for the different boxes within a basin shelf, which is motivated in Appendix B. Thus, for example, the box  $B_1$  adjacent to the grounding line interacts with all ice shelf grid cells with  $0 \leq r \leq 1 - \sqrt{(n_D - 1)/n_D}$ . Figure 3 shows an example of the ocean box areas for Antarctica. PICO does currently not account for melting along vertical ice cliffs, as for example the termini of some Greenland outlet fjords.

## 20 2.4 Implementation in the Parallel Ice Sheet Model

- PICO is implemented in the open-source Parallel Ice Sheet Model (PISM: Bueler and Brown, 2009; Winkelmann et al., 2011). In the 3d, thermo-mechanically coupled, finite-difference model, ice velocities are computed through a superposition of the shallow approximations for the slow, shear-dominated flow in ice sheets (Hutter, 1983, SIA) and the fast, membrane-like flow in ice streams and ice shelves (Morland, 1987, SSA). In PISM, the grounding lines (diagnosed via the flotation criterion) and ice fronts evolve freely. Grounding line movement has been evaluated in the model intercomparison project MISMP3d (Pattyn et al., 2013; Feldmann et al., 2014).

- Time-stepping in PICO is the same as in PICO is synchronously coupled to the ice-sheet model, i.e., they use the same adaptive time steps. The cavity model provides sub-shelf melt rates and temperatures at the ice-ocean boundary to PISM, with temperatures being at the in-situ freezing point. PISM supplies the evolving ice-shelf geometry to PICO, which in turn updates adjusts in each time step the ocean box geometry to the ice-shelf geometry as described in Sect. 2.3.

PICO computes the melt rates progressively over the ocean boxes, independently for each basin~~ice shelf~~. Since the ice-sheet model has a much higher resolution, each ocean box interacts with a number of ice shelf grid cells. PICO applies the analytic solutions of the system of governing equations summarized in Sect. 2.1 and 2.2 locally to the ice model grid as detailed below. Model parameters that are varied between the experiments are the effective turbulent heat exchange velocity  $\gamma_T^*$  from the melt parametrization described in Sect. 2.2 and the overturning coefficient  $C$  described in Sect. 2.1. ~~Despite the distinction into basins, the same~~The two parameter values are applied ~~for to~~for to the entire ice-sheet.

Input for PICO in the ocean reservoir box  $B_0$  is data from observations or large-scale ocean models in front of the ice shelves. Temperature  $T_0$  and salinity  $S_0$  are averaged at the depth of the bathymetry in the continental shelf region. In box  $B_1$  adjacent to the grounding line, PICO solves the system of governing equations in each ice grid cell  $(x, y)$  to attain the overturning flux  $q(x, y)$ , temperature  $T_1(x, y)$ , salinity  $S_1(x, y)$  and the melting  $m_1(x, y)$  at its ice-ocean interface (given by the local solution of ~~Eq~~Eqs. 3, ~~Eq. A12, Eq. A8 and Eq. A12, A8 and~~ 8, respectively). The model proceeds progressively from box  $B_k$  to box  $B_{k+1}$  to solve for sub-shelf melt rate  $m_{k+1}(x, y)$ , ambient ocean temperature  $T_{k+1}(x, y)$  and salinity  $S_{k+1}(x, y)$  (given by the local solution of ~~Eqn~~Eqs. 13, ~~Eqn. A13 and Eqn. A13 and~~ A8, respectively) based on the previous solutions  $S_k$  and  $T_k$  in box  $B_k$  and conditions at the ice-ocean interface. PICO provides the boundary conditions  $T_k$  and  $S_k$  to box  $B_{k+1}$  as the average over the ice-grid cells ~~along the boundary between boxes within box~~  $B_k$  and  $B_{k+1}$  ensuring a smooth transition of sub-shelf melt rates and ocean water properties, *i.e.*,

$$T_k = \langle T_k(x, y) \text{ with } (x, y) \text{ in } B_k \text{ and adjacent to } B_{k+1} \rangle \quad (12)$$

and analogously for  $S_k$ , where  $\langle \rangle$  denotes the average.

The overturning is solved in Box  $B_1$  and given by  ~~$q = \langle q(x, y) \text{ with } (x, y) \text{ in } B_1 \text{ and adjacent to } B_2 \rangle$~~   $q = \langle q(x, y) \text{ with } (x, y) \text{ in } B_1 \rangle$ . Melt rates in box  $B_k$  are computed using the local overburden pressure  $p_k(x, y)$  in each ice shelf grid cell that is given by the weight of the ice column provided by PISM, *i.e.*,

$$m_k(x, y) = -\frac{\gamma_T^*}{\nu\lambda} (aS_k(x, y) + b - cp_k(x, y) - T_k(x, y)). \quad (13)$$

This reflects the pressure dependence of heat available for melting and leads to a depth-dependent melt rate pattern within each box. The implications for energy and mass conservation are discussed in Sect. 3.2 and Sect. 4.

### 25 3 Results for present-day Antarctica

We apply PICO to compute sub-shelf melt rates for all Antarctic ice shelves under present-day conditions. ~~Based on Zwally et al. (2012), we determine 19 basins of the Antarctic Ice Sheet and extend these to the attached ice shelves and the surrounding Southern Ocean (Fig. 2). We combine drainage sectors feeding the same ice shelf, e.g., all contributory inlets to Filchner-Ronne or Ross Ice Shelves. We also consolidate the basins 'IceSat21' and 'IceSat22' (Pine Island Glacier and Thwaites Glacier) as well as 'IceSat7' and 'IceSat8' in East Antarctica. Ocean conditions in box  $B_0$  are~~ Oceanic input for each ice shelf is given by observations of temperature (converted to potential temperature) and salinity (converted to practical salinity) of the water masses occupying the sea floor on the continental shelf (Schmidtko et al., 2014), averaged over the time period 1975 to

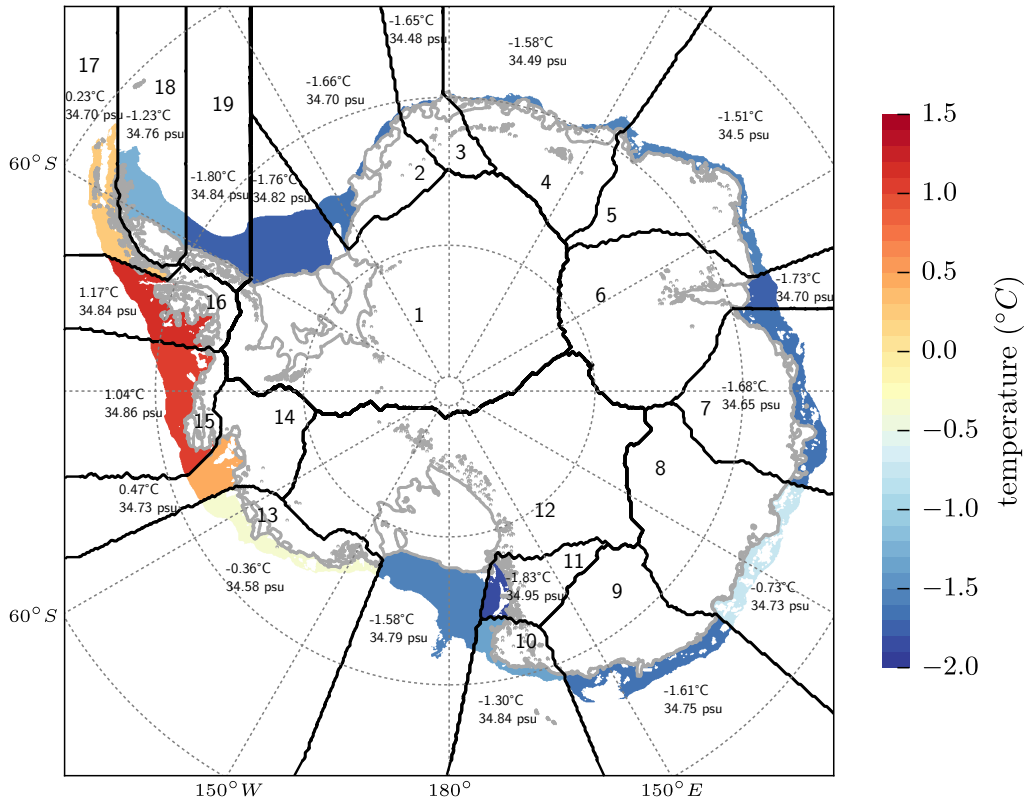


**Figure 2.** PICO input for Antarctic basins. The ice sheet, ice shelves and the surrounding Southern Ocean are split into 19 basins that are based on Zwally et al. (2012) and indicated by black contour lines and labels. For each [basin](#), the governing equations are solved separately with the respective oceanic boundary conditions. [For ice shelves that cross basin boundaries, the input is averaged, weighted with the fractional area of the shelf within the corresponding basin.](#) Numbers show the temperature and salinity input in [box  \$B\_0\$](#)  each basin, obtained by averaging observed properties of the ocean water in front of the ice shelf cavities at depth of the continental shelf (Schmidtke et al., 2014), indicated by the color shading. Grey lines show Antarctic grounding lines and ice shelf fronts (Fretwell et al., 2013).

2012. [Water masses within an ice shelf cavity originate from source regions: Neglecting ocean dynamics, we approximate these by averaging ocean properties on the depth of the continental shelf within regions that are chosen to encompass areas of similar, large-scale ocean conditions.](#) Oceanic input is given for 19 basins of the Antarctic Ice Sheet, which are based on Zwally et al. (2012) and extended to the attached ice shelves and the surrounding Southern Ocean (Fig. 2). For each ice shelf, temperature  $T_0$  and salinity  $S_0$  in box  $B_0$  are obtained by averaging the basin input weighted with the fractional area of the shelf within the corresponding basin. Figure 2 shows the basin-mean ocean temperature (shadings and numbers) and salinity (numbers) used as [input values](#).<sup>3</sup>

<sup>3</sup>We combine drainage sectors feeding the same ice shelf, e.g., all contributory inlets to Filchner-Ronne or Ross Ice Shelves. We also consolidate the basins 'IceSat21' and 'IceSat22' (Pine Island Glacier and Thwaites Glacier) as well as 'IceSat7' and 'IceSat8' in East Antarctica.

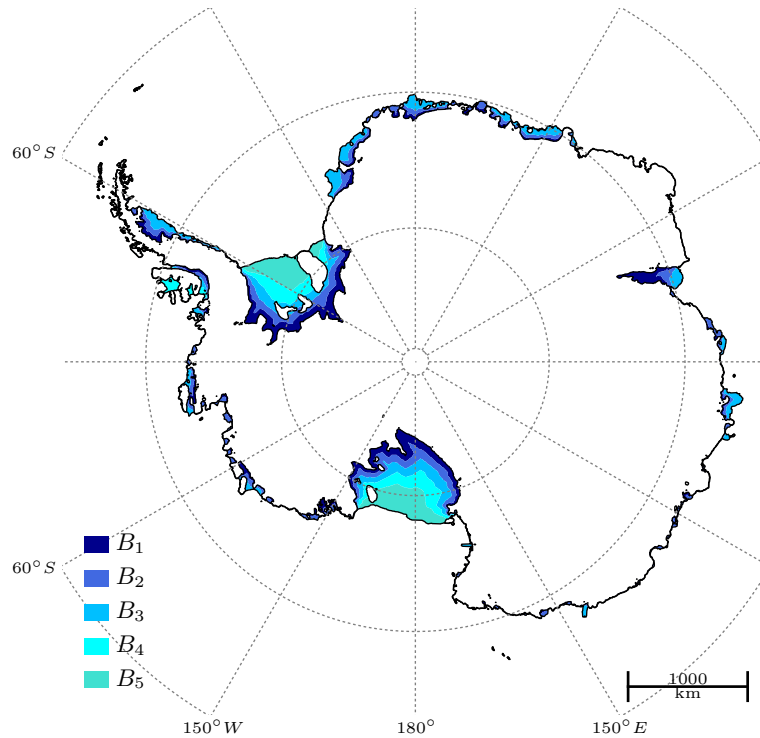


**Figure 3.** Extent of PICO ocean boxes for Antarctic ice shelves. Most ice shelves are split into two, three or four ocean boxes interacting with the ice cells on a much higher resolution. The largest ice shelves, Filchner-Ronne and Ross, have five ocean boxes. One ocean box typically corresponds to many ice shelf grid cells.

Here, we use  $n_{\max} = 5$  from which PICO determines the number of ocean boxes in each [basin-shelf](#) via Eq. 9. Figure 3 displays the resulting extent of the ocean boxes for Antarctica, ordered in elongated bands beneath the ice shelves. For the large ice-shelf cavities of Filchner-Ronne and Ross the ice-ocean boundary is divided into five ocean boxes while smaller ice shelves have two to four boxes (see Table 2). Introducing more than five ocean boxes has a negligible effect on the melt rates, as discussed in Sect. 3.2.

To validate our model, we run diagnostic simulations with PISM+PICO based on bed topography and ice thickness from BEDMAP2 (Fretwell et al., 2013) mapped to a grid with 5 km horizontal resolution. Diagnostic simulations allow us to assess the sensitivity of the model to the parameters  $C$  and  $\gamma_T^*$  and to the number of boxes  $n_{\max}$  as well as the ice model resolution. [Transient behavior is exemplary shown in a simulation starting from an equilibrium state of the Antarctic Ice Sheet forced with ocean temperature changes, see Supplementary Video S.1 and Sect. 3.3.](#)

### 3.1 Sensitivity to model parameters $C$ and $\gamma_T^*$

We test the sensitivity of sub-shelf melt rates to the model parameters for overturning strength  $C \in [0.1, 9] \text{ Sv m}^3 \text{ kg}^{-1}$  and the effective turbulent heat exchange velocity  $\gamma_T^* \in [5 \times 10^{-6}, 1 \times 10^{-4}] \text{ m s}^{-1}$ . These ranges encompass the values identified

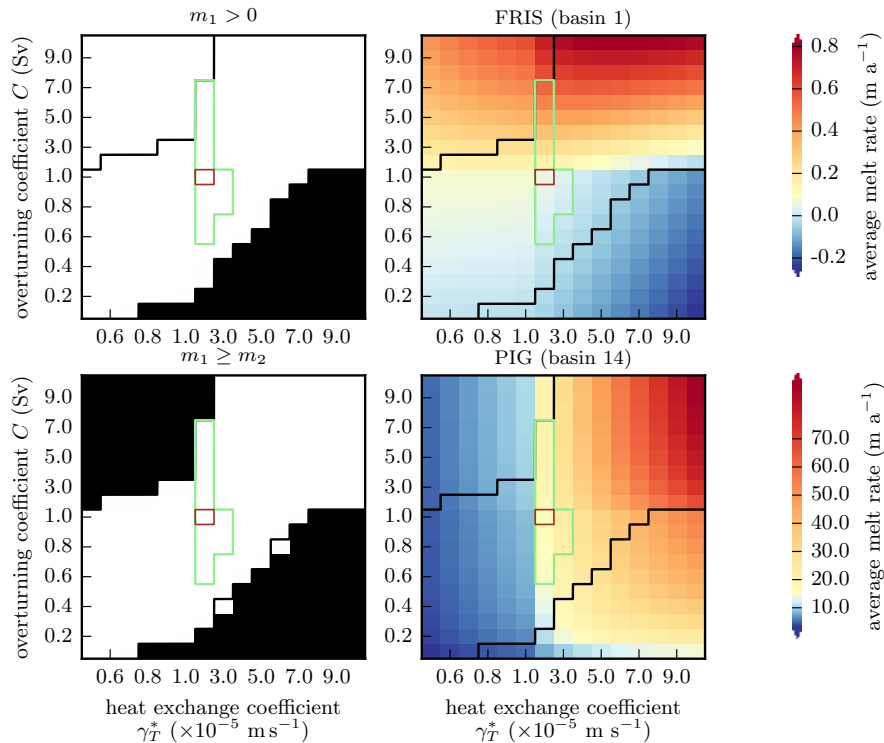


**Figure 4.** Sensitivity of PICO sub-shelf melt rates to the overturning coefficient  $C$  and the effective turbulent heat exchange coefficient  $\gamma_T^*$ . Black contour indicates the valid range of parameters, all other parameter combinations are excluded by one of the following criteria: **(Upper left)** No freezing may occur in the first ocean box  $\neg$ ; **(Lower upper left)**, mean basal melt rates must decrease between the first and second ocean box  $\neg$ ; **(Upper right lower left)**, Green contour indicates the valid range of parameters where the following quantitative constraints are additionally met: mean basal melt rates for Filchner-Ronne Ice Shelf should be within the range of  $0.05$ - $0.01$   $\text{m a}^{-1}$   $\neg$ ; **(Lower upper right)**, mean basal melt rates for the basin containing Pine Island Glacier Ice Shelf should be within the range of  $10$ - $10.0$   $\text{m a}^{-1}$  to  $20$ - $25.0$   $\text{m a}^{-1}$  (lower right). The best-fit parameters (brown contour) minimize the root mean square error of mean melt rates to observations for both ice shelves.

in OH10, discussed further in Appendix A. The same parameters for  $C$  and  $\gamma_T^*$  are applied to all basins shelves. We validate the results by the following sieve criteria qualitative criteria (1) and (2) as well as the quantitative constraints (3) and (4), summarized in Fig. 4:

- Criterion (1):* Freezing must not occur in the first box  $B_1$  of any basin, *i.e.*, the ocean box closest to the grounding line.
- 5 Freezing in box  $B_1$  would increase ambient salinity, and since the overturning circulation in ice-shelf cavities is mainly haline-driven, the circulation would shut down, violating the model assumption  $q > 0$  (see Sect. 2). As shown in the upper left panel of Fig. 4, the condition is not met for a combination of relatively high turbulent heat exchange and relatively low overturning parameters. In such cases, freezing near the grounding line occurs because of the strong heat exchange between the ambient

ocean and the ice-ocean boundary in box  $B_1$  that cannot be balanced by the resupply of heat from the open ocean through overturning.

*Criterion (2):* Sub-shelf melt rates must decrease between the first and second box for each basin. This condition is based on general observations of melt-rate patterns and on the assumption that ocean water masses move consecutively through the boxes and cool down along the way, as long as melting in these boxes outweighs freezing. As shown in the lower left panel in Fig. 4, this condition is violated for either high overturning and low turbulent heat exchange or, vice versa, low overturning and high turbulent heat exchange. An appropriate balance between the strength of these values is hence necessary for a realistic melt rate pattern.

If criterion (1) or (2) fails, basic assumptions of PICO are violated. Thus, we choose the model parameters  $\gamma_T^*$  and  $C$  such that both criteria are strictly met. The following quantitative criteria, observational constraints (3) and (4) compare modeled average melt rates with observations and thus depend on our choice of valid ranges. We choose basin 1 and 14 Filchner-Ronne Ice Shelf and the ice shelf adjacent to Pine-Island Glacier to further constrain our model parameters for Antarctica. Basin 1 contains the Filchner-Ronne Ice Shelf and basin 14 the ice shelves in the Amundsen Sea. These two basins These shelves represent two different types of ice shelves regarding both the mode of melting and the ice-shelf size.

*Criterion* Observational constraint (3): Average melt rates in Filchner-Ronne Ice Shelf comply with the classification of a “cold” cavity and lie between 0.05-0.01  $\text{m a}^{-1}$  and  $1.0 \text{ m a}^{-1}$  (Fig. 4, upper right panel).

*Criterion* Observational constraint (4): In the Amundsen basin, for For Pine Island Glacier, with “warm” ocean conditions, average melt rates lie between 10 and 20  $\text{m a}^{-1}$  and 25  $\text{m a}^{-1}$  (Fig. 4, lower right panel).

Generally, an increase in overturning strength  $C$  will supply more heat and thus yield higher melt rates, especially for the large and “cold” ice shelves like Filchner-Ronne. In the valid parameter range, larger Larger  $C$  leads to higher melt rates also in the smaller and “warm” basins like Pine-Island Glacier Ice Shelf but the effect is less pronounced. In contrast, the turbulent heat exchange alters melting particularly in basins with small ice shelves while it might decrease melt rates in large ice shelves with “cold” cavities. Hence, modeled melting in the Filchner-Ronne basin Ice Shelf is dominated by overturning while in the Amundsen region melting is dominated by turbulent exchange across the ice-ocean boundary layer. For three different parameter combinations, the resulting spatial patterns of melt rates in the Filchner-Ronne and Pine Island regions are displayed in Fig. S.1.

All of the above criteria restrict the parameter space to a bounded set with lower and upper limits as depicted by the contour line green contour lines in Fig. 4. We determine a best-fit pair of parameters which minimizes the root mean square error of average melt rates for both ice shelves. The valid range of model parameters with  $C$  around 1 and  $\gamma_T^*$  around  $2 \times 10^{-5}$  the best-fit parameters with  $C = 1 \text{ Sv m}^3 \text{ kg}^{-1}$  and  $\gamma_T^* = 2 \times 10^{-5} \text{ m a}^{-1}$  compares well with those parameters found in OH10 and Holland and Jenkins (1999).

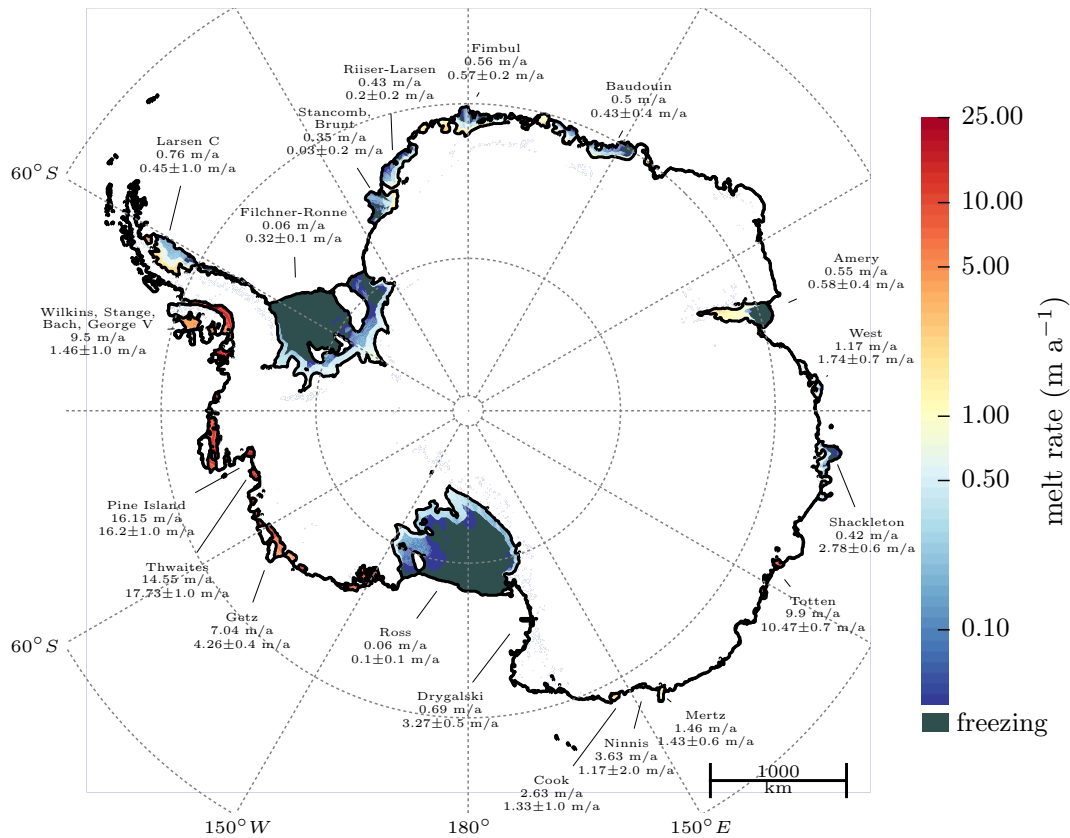


**Figure 5.** Sub-shelf melt rates for present-day Antarctica computed with PISM+PICO. For each basin, the mean melt rate per ice shelf (upper numbers) is compared to the observed range-melt rates (lower numbers with uncertainty ranges) from Rignot et al. (2013). In the model, the same parameters  $\gamma_T^* = 2 \times 10^{-5} \text{ m s}^{-1}$  and  $C = 1 \text{ Sv m}^3 \text{ kg}^{-1}$  are applied to all ice shelves around Antarctica. The respective oceanic boundary conditions are shown in Fig. 2. Ice geometry and bedrock topography are from the BEDMAP2 data set on 5km resolution (Fretwell et al., 2013). Refreezing occurs in some parts of the larger shelves like Filchner-Ronne and Ross.

### 3.2 Diagnostic melt rates for present-day Antarctica

Using the best-fit values  $C = 1 \text{ Sv m}^3 \text{ kg}^{-1}$  and  $\gamma_T^* = 2 \times 10^{-5} \text{ m s}^{-1}$  found in Sect. 3.1, we apply PICO to present-day Antarctica, solving for sub-shelf melt rates and water properties in the ocean boxes. This model simulation is referred to as “reference simulation” hereafter.

- 5 The average melt rates computed with PICO range from ~~0.07~~0.06  $\text{m a}^{-1}$  under the Ross Ice Shelf to ~~12.13~~16.15  $\text{m a}^{-1}$  for the Amundsen Region (Fig. 5). Generally consistent with the model assumptions, melt rates are highest in the vicinity of the grounding line and decrease towards the calving front. In some regions of the large ice shelves, refreezing occurs, e.g., towards the center of Filchner-Ronne or Amery ice shelves. The melt pattern also depends on the local pressure melting temperature, which is a function of the local ice thickness. Thus, in some boxes freezing occurs in regions of relatively thin ice while

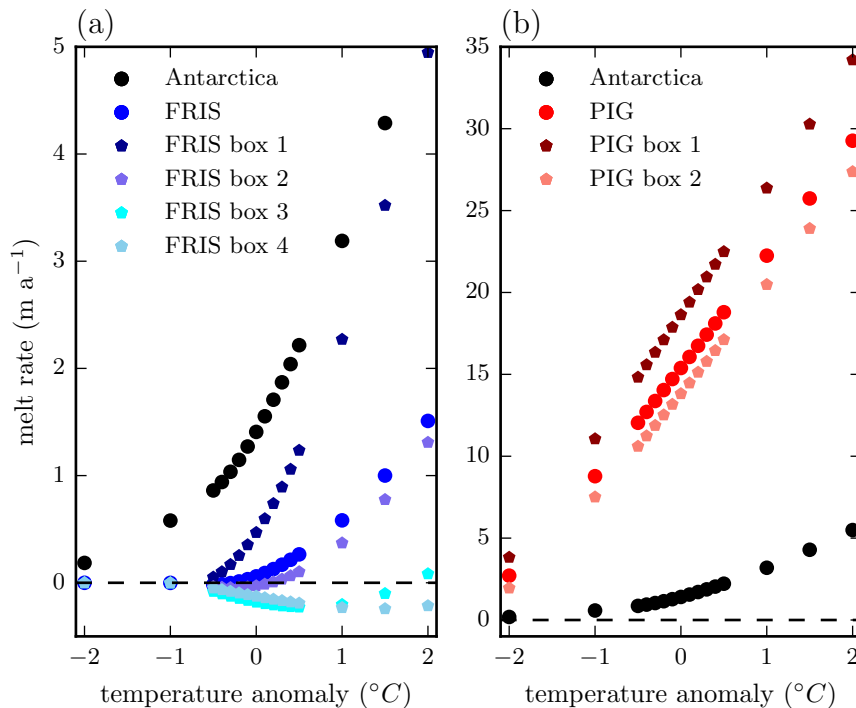


**Figure 6.** Sensitivity of PICO sub-shelf melt rates to ocean temperature changes for entire Antarctica (black), Filchner-Ronne Ice Shelf (blue) and ~~the basin containing~~ Pine Island Glacier Ice Shelf (red). Ocean input temperatures are varied by  $0.1^{\circ}\text{C}$  up to  $2^{\circ}\text{C}$ . Melting depends quadratically on temperature for “cold” cavities like the one adjacent to Filchner-Ronne, and linearly for “warm” cavities like the ones in the Amundsen Region.

~~melting occurs in regions where the ice shelf is thicker.~~ Thus, melt rates are highest where the shelf is thickest, *i.e.*, near the grounding lines within box  $B_1$ . Furthermore, freezing and melting can occur in the same box determined by local ice shelf thickness. For the vast majority of ice shelves, the ~~modeled-modelled~~ average melt rates compare well with the observed ranges derived from Table 1 in Rignot et al. (2013). An exception are ~~the two basins containing Abbot and Cosgrove ice shelves~~ (basin 15) as well as Wilkins and Stange ice shelves (in basin 16) with average ~~modeled-modelled~~ melt rates of ~~11.39 and 8.87~~ 9.50 respectively  $\text{m a}^{-1}$ , which is much higher than the observed range of ~~1.8–3.4 and 2.39–4.18~~  $1.46 \pm 1.0$   $\text{m a}^{-1}$ . This is most likely due to the ocean temperature input for ~~these basins (1.04 and 1.16~~ this basin (1.17  $^{\circ}\text{C}$ , see Fig. 2) which is higher than for the basin containing Pine Island located nearby ( $0.47^{\circ}\text{C}$ , basin 14), explaining why the melt rates are of the same order of magnitude in these basins. Modification of water masses flowing into the shelf cavities, not captured by PICO, might explain the low observed melt rates in ~~basins 15 and 16~~ this area despite the relatively high ocean temperatures.

For all ~~basins~~ ice shelves, ocean temperatures and salinities consistently decrease in overturning direction, *i.e.*, from the ocean reservoir box  $B_0$  to the last box adjacent to the ice front  $B_n$ , as shown in Table 2. Most ~~basins~~ shelves contain small areas ~~in~~

**Table 2.** Results from the reference simulation as displayed in Fig. 5.

| Ice shelf                        | $b_n$ | $T_0$ | $S_0$ | $T_n$ | $S_n$ | $\Delta T$ | $\Delta S$ | $q$  | $m$   | $m_{observed}$   |
|----------------------------------|-------|-------|-------|-------|-------|------------|------------|------|-------|------------------|
| Larsen C                         | 3     | -1.33 | 34.60 | -2.02 | 34.28 | -0.69      | -0.32      | 0.16 | 0.76  | $0.45 \pm 1.00$  |
| Wilkins, Stange, Bach, George VI | 4     | 1.17  | 34.67 | -1.41 | 33.48 | -2.58      | -1.19      | 0.32 | 9.50  | $1.46 \pm 1.00$  |
| Pine Island                      | 2     | 0.46  | 34.55 | -0.49 | 34.12 | -0.94      | -0.44      | 0.17 | 16.15 | $16.20 \pm 1.00$ |
| Thwaites                         | 2     | 0.46  | 34.55 | -0.62 | 34.06 | -1.07      | -0.50      | 0.13 | 14.55 | $17.73 \pm 1.00$ |
| Getz                             | 3     | -0.37 | 34.41 | -1.63 | 33.83 | -1.26      | -0.58      | 0.23 | 7.04  | $4.26 \pm 0.40$  |
| Drygalski                        | 3     | -1.84 | 34.78 | -2.03 | 34.69 | -0.19      | -0.09      | 0.02 | 0.69  | $3.27 \pm 0.50$  |
| Cook                             | 2     | -1.62 | 34.58 | -1.94 | 34.43 | -0.32      | -0.15      | 0.05 | 2.63  | $1.33 \pm 1.00$  |
| Ninnis                           | 2     | -1.62 | 34.58 | -1.88 | 34.45 | -0.26      | -0.12      | 0.04 | 3.63  | $1.17 \pm 2.00$  |
| Mertz                            | 3     | -1.62 | 34.58 | -1.99 | 34.40 | -0.38      | -0.17      | 0.04 | 1.46  | $1.43 \pm 0.60$  |
| Totten                           | 2     | -0.68 | 34.57 | -1.26 | 34.29 | -0.59      | -0.27      | 0.13 | 9.90  | $10.47 \pm 0.70$ |
| Shackleton                       | 3     | -1.69 | 34.48 | -2.03 | 34.32 | -0.34      | -0.16      | 0.07 | 0.42  | $2.78 \pm 0.60$  |
| West                             | 2     | -1.69 | 34.48 | -2.01 | 34.33 | -0.32      | -0.15      | 0.07 | 1.17  | $1.74 \pm 0.70$  |
| Amery                            | 3     | -1.72 | 34.53 | -2.16 | 34.33 | -0.43      | -0.20      | 0.16 | 0.55  | $0.58 \pm 0.40$  |
| Baudouin                         | 3     | -1.55 | 34.33 | -2.06 | 34.09 | -0.51      | -0.23      | 0.12 | 0.50  | $0.43 \pm 0.40$  |
| Fimbul                           | 3     | -1.57 | 34.32 | -2.06 | 34.10 | -0.49      | -0.23      | 0.10 | 0.56  | $0.57 \pm 0.20$  |
| Riiser-Larsen                    | 3     | -1.66 | 34.53 | -2.06 | 34.34 | -0.40      | -0.19      | 0.09 | 0.43  | $0.20 \pm 0.20$  |
| Stancomb, Brunt                  | 3     | -1.66 | 34.53 | -2.01 | 34.37 | -0.35      | -0.16      | 0.08 | 0.35  | $0.03 \pm 0.20$  |
| Filchner-Ronne                   | 5     | -1.76 | 34.65 | -2.19 | 34.45 | -0.43      | -0.20      | 0.21 | 0.06  | $0.32 \pm 0.10$  |
| Ross                             | 5     | -1.58 | 34.63 | -2.12 | 34.38 | -0.53      | -0.25      | 0.17 | 0.06  | $0.10 \pm 0.10$  |

The number of boxes for each ice shelf is given by  $b_n$ ,  $T_0$  ( $S_0$ ) is the temperature (salinity) in ocean box  $B_0$ ,  $T_n$  ( $S_n$ ) the temperature (salinity) averaged over the ocean box at the ice shelf front,  $\Delta T = T_n - T_0$  and  $\Delta S = S_n - S_0$ .  $m$  is the average sub-shelf melt rate,  $m_{observed}$  the observed melt rates from Rignot et al. (2013).  $q$  is the overturning flux. Unit of temperatures is  $^{\circ}\text{C}$ , salinity is given in PSU, melt rates in  $\text{m a}^{-1}$  and overturning flux in Sv.

~~which ocean water freezes to the ice shelf base, with accretion~~ with a maximum rate of  ~~$-0.63$~~  ~~$-1.22$~~   $\text{m a}^{-1}$  for the Amery Ice Shelf, see Table S.1. No freezing occurs at the Western Antarctic Peninsula nor in the Amundsen and Bellingshausen Seas. A detailed map of sub-shelf melt rates in this region as well as for Filchner-Ronne Ice Shelf can be found in [the middle panels of Fig. S.1](#). For the Filchner-Ronne Ice Shelf melt rates vary between  ~~$-0.49$~~  ~~$-0.67$~~   $\text{m a}^{-1}$  and  $1.76 \text{ m a}^{-1}$  and for ~~the basin~~ ~~containing~~ Pine Island Glacier, melt rates range from  ~~$8.87$~~  ~~$12.39$~~   $\text{m a}^{-1}$  to  ~~$18.85$~~  ~~$21.01$~~   $\text{m a}^{-1}$ .

[PICO tends to smooth out melt rate patterns, see Fig. S.4: For Filchner-Ronne and Ross ice shelves the deviations in observed melt rates \(Moholdt et al., 2016\) from the average melting are larger than the deviations modelled in PICO. The box-wide averages compare well and are at the same order of magnitude for both ice shelves, except for modelled accretion in the later boxes towards the shelf front which is not reflected in the observations. This disagreement might be explained by the fact that the overturning circulation in the model cannot reach neutral density and detach from the ice-shelf base while flowing towards the shelf front.](#)

Aggregated over all Antarctic ice shelves, the total melt flux is ~~1,299–1,718~~  $\text{Gt a}^{-1}$ , close to the observed estimate of  $1,500 \pm 237 \text{ Gt a}^{-1}$  (Rignot et al., 2013). Overturning fluxes in our reference simulation range from ~~0.03–0.02~~ Sv for the ~~basin containing the small ice shelves Drygalski and Nansen to 0.35~~ small Drygalski Ice Shelf to 0.32 Sv along the Western Antarctic Peninsula for Wilkings, Stange, Bach and George VI ice shelves. Because these are treated in PICO as one ice shelf and they have a high input temperature, these ice shelves reach together this high overturning value. The second highest value of 0.23 Sv is found for Getz Ice Shelf in the Bellingshausen Sea. These overturning fluxes compare well with the estimates in OH10.

PICO solves the system of governing equations locally in each ice-model grid cell and calculates input for each ocean box as an average ~~along the boxes boundary over the previous box~~ as described in Sect. 2.4. Due to this model assumptions and because temperature, salinity, overturning and melting are non-linear functions of pressure in the first box (Eqn. A12), mass and energy are a-priori not perfectly conserved. In Table S.1, we compare (within ~~each basin individual shelves~~) heat fluxes into the ice shelf cavities with the heat flux out of the cavities into the ocean and the latent heat flux for melting. For the whole of Antarctica, the deviation in heat flux is ~~–282.15–403.63~~  $\text{GJ s}^{-1}$  which is equivalent to ~~2.0%–2.2%~~ of the latent heat flux for melting. The per-basin deviations are generally low (~~<15% < 5%~~), except around ~~Amery and Filchner-Ronne ice shelves. This can be explained by an underestimation of the overturning in these particular basins, which is due to the computation of the overturning flux  $q$  along the boundary between boxes  $B_1$  and  $B_2$  (at a depth of 423 and 700, respectively) instead of using the average shelf depth in  $B_1$  (which is 671 and 839). Summed over all Antarctic ice shelves, the error in overturning introduced by this choice of implementation is however small. the large Filchner-Ronne and Ross ice shelves.~~ In PICO we assume  $q$  to be constant, neglecting changes due to melt water input along the shelf base. This melt water input amounts to ~~3.17%–3.06%~~ or less of the overturning flux within ~~each basin, and 1.4% ice shelves, and 0.62%~~ for the entire continent, discussed in Sect. 2.1.

Melt rates are strongly affected by changes in the ambient ocean temperatures, see Fig. 6. The dependence is approximately linear for high and quadratic for lower ambient ocean temperatures. This relationship is similar to the one observed in OH10 and as expected from the governing equations. In Pine Island Glacier, melt rates increase by approximately  $6 \text{ m a}^{-1}$  per degree of warming. Changes in the ice-sheet model resolution have little effect on the resulting melt rates (Fig. S.2). For increasing the maximum number of boxes  $n_{\text{max}}$ , average melt rates converge to almost constant values for  $n_{\text{max}} \geq 5$  within all basins, compare Fig. S.3.

### 3.3 Transient evolution of PICO boxes and melt rates

PICO is capable of adjusting to changing ice-shelf geometries and migrating grounding lines. We demonstrate its behaviour as a module in PISM in a transient simulation: Based on an Antarctic equilibrium state at 8km resolution comparable to the state submitted to initMIP (Nowicki et al., 2016), we run PISM+PICO over time with a simple temperature forcing applied: Starting from equilibrium conditions, ocean temperatures increase linearly over 50 years until an ocean-wide warming of  $1^\circ\text{C}$  is reached. It is then held constant over the next 250 modeled years. The Supplementary Video S.1 shows the temporal evolution of the ocean temperature input for the ice shelf adjacent to Pine Island Glacier as well as the Filchner-Ronne Ice Shelf. The ocean temperature increase enhances the sub-shelf melting for both ice shelves, especially in the first box. Ice-shelf thinning reduces buttressing and causes the grounding lines to retreat with the ocean boxes adjusting accordingly.

## 4 Discussion

PICO models the dominant vertical overturning circulation in ice shelf cavities and translates ocean conditions in front of the ice shelves, either from observations or large-scale ocean models, into physically-based sub-shelf melt rates. For present-day ocean fields and ice-shelf cavity geometries, PICO as an ocean module in PISM reproduces average melt rates of the same order of magnitude as observations for ~~all Antarctic basins~~ most Antarctic ice shelves. With a single combination of overturning parameter  $C$  and effective turbulent heat exchange parameter  $\gamma_T^*$  applied to all ~~basins~~ shelves, a wide range of melt rates for the different ice shelves is obtained, reproducing the large-scale patterns observed in Antarctica. The results are consistent across different ice-sheet and cavity model resolutions. Additionally, PICO reproduces the common pattern of maximum melt close to the grounding line and decreasing melt rates towards the ice shelf front, eventually with re-freezing in the shallow parts of the large ice shelves. The governing model equations are solved for individual grid cells of the ice sheet model (and not for each ocean box with representative depth value), which ~~yields a comparably high resolution of the obtained~~ allows spatial variability in the resulting melt rate field at comparatively smaller scale. PICO can adapt to evolving cavities and is applicable to ice shelves in two horizontal dimensions. It is hence suited as a sub-shelf melt module for ice-sheet models.

~~In the underlying equations, transversal transport within~~ Yet PICO is a coarse model designed as an ocean coupler for large-scale ice-sheet models. It is based on the OH10 model and hence shares some simplifying assumptions with that model: PICO does not resolve ocean dynamics besides the parametrized vertical overturning circulation in the ice shelf cavities which is given by one value for each ice shelf. The underlying equations of PICO do not resolve horizontal ocean circulation in the ice shelf cavities ~~; e.g., due to Coriolis force is not represented. Seasonal melt rate driven by the Coriolis force nor seasonal melt~~ variation due to intrusion of warm water from the calving front during Austral summer ~~is also not included in the model.~~ ~~Boundary conditions as input for the next following ocean box are evaluated as mean along the inter-box boundary, which permits a smooth distribution of modeled melt rates across the ice shelves. For the entire continent, the relative error in the overturning flux introduced by averaging along the boundary as compared to the mean over the entire ocean box is 3.5%. For the estimated heat fluxes, the relative error is lower than 2.0% of the latent heat flux due to sub-shelf melting. Regarding mass conservation the relative error introduced by assuming the overturning to be constant along the boxes is below 1.4%. Hence,~~ we do not expect that horizontal variations or small scale patterns of basal melt are accurately captured in PICO. Due to the box model formulation, maximum melting in PICO is found directly at the grounding line and not slightly downstream as seen in the high-resolution coupled ice-ocean simulation by, e.g., De Rydt and Gudmundsson (2016). We find that PICO tends to produce smoother melt rate patterns than observed, though the box-wide averages are in good agreement with observations. The effect on ice dynamics of small-scale differences in melt patterns in relation to the large-scale mean melt fluxes is not well established yet and needs further investigation. Following OH10, meltwater does not contribute to the volume flux in the cavity in PICO, introducing a minor error regarding mass conservation. The relative error regarding mass conservation is however small and below 0.7% of the total overturning strength ~~. We hence consider our choice of model simplifications as justified regarding the associated small errors introduced in the heat and mass balances for our reference simulation.~~

in our reference run. A necessary condition for the box model to work is further the assumption of melting in box  $B_1$  which is consistent with the majority of available observations. In PICO, melt rates show a quadratic dependency on ocean temperature input for lower temperatures, *e.g.*, in the Filchner-Ronne basins, and a rather linear dependency for higher temperatures, *e.g.*, in the Amundsen basin. This is consistent with the results from OH10 and the implemented melting physics assuming a constant coefficient for turbulent heat exchange. In contrast, Holland et al. (2008b) employ a dependency of the turbulent heat exchange coefficient on the velocity of the overturning circulation, suggesting melt rates to respond quadratically to warming of the ambient ocean water. Here we follow the approach taken in OH10.

Differently from the OH10 model and relying on much longer timescales of ice dynamics in comparison to ocean dynamics, PICO assumes the overturning circulation to be in steady state. In their analysis, OH10 find unstable vertical water columns to occur only transiently, and hence for PICO a stable stratification of the vertical water column is assumed. Under these conditions, diffusive transport between the boxes is generally small in OH10 and it is hence omitted in PICO. Because PICO also does not consider vertical variations in ambient ocean density, under-ice flow is prevented from reaching neutral density and detaching from the ice-shelf base on its way towards the shelf front. The spatial pattern of melting closer to the calving front of cold ice shelves may in such cases be not represented well.

PICO input is determined by averaging bottom temperatures and salinities over the continental shelf, this is done for 19 different basins. Hence PICO - as a coarse model - misses the nuances of how ocean currents transport and modify CDW over the regions being averaged. The procedure to determine melt rates in PICO is based on the assumption that ocean water that is present on the continental shelf can access the ice shelf cavities and reach their grounding lines. This implies for example, that barriers like sills that may prevent intrusion of warm CDW are not accounted for and might explain why PICO melting is too high for the ice shelves located along the Southern Antarctic Peninsula. Such phenomena could be tested by varying the ocean input of PICO by evolving the temperature and salinity outside of the cavity over time. Because of the dependence of sub-shelf melting on the local pressure of the ice column above, the model is not fully energy conserving. For the estimated heat fluxes, the relative error is lower than 2.2% of the latent heat flux due to sub-shelf melting. Hence, we consider our choice of model simplifications as justified, since it introduces small errors in the heat and mass balances in our reference simulation.

PICO is computationally ~~very~~-fast, as it uses analytic solutions of the equations of motion with a small number of boxes along the ice shelf. As boundary conditions for PICO are aggregated based on predefined regional basins, the model can act as an efficient coupler of large-scale ice-sheet and ocean models. For this purpose, heat flux into the ice should be added to the boundary layer melt formulation.

## 5 Conclusions

The Antarctic Ice Sheet plays a vital role in modulating global sea level. The ice grounded below sea level in its marine basins is susceptible to ocean forcing and ~~responds-might respond~~ nonlinearly to changes in ocean boundary conditions (Mercer, 1978; Schoof, 2007). We therefore need carefully estimated conditions at the ice-ocean boundary to better constrain the dynamics of the Antarctic ice and its contribution to sea-level rise for the past and the future.

The PICO model presented here provides a physics-based yet efficient approach for estimating the ocean circulation below ice shelves and the heat provided for ice shelf melt. The model extends the one-horizontal-dimensional ocean box model by OH10 to realistic ice shelf geometries following the shape of the grounding line and calving front. PICO is a comparably simple ~~and fast~~ alternative to full ocean models, but goes beyond local melt parameterizations, which do not ~~fully reflect~~ account for the circulation below ice shelves. ~~We validated the model using~~ We find a set of possible parameters for present-day ocean conditions and ice geometries ~~. PICO accurately which yield PICO melt rates in agreement with average melt rate observations. PICO qualitatively~~ reproduces the general pattern of ice shelf melt, with high melting at the grounding line and low melting or refreezing towards the calving front. Its sensitivity to changes in input ocean temperatures and model parameters is comparable to earlier estimates (Holland and Jenkins, 1999; Olbers and Hellmer, 2010). The model accurately captures the large variety of observed Antarctic melt rates using only two calibrated parameters ~~that are valid for the whole ice sheet~~ applied to all ice shelves.

The ocean models that are part of the large Earth system and global circulation models do not yet resolve the circulation below ice shelves. PICO is able to fill this gap and can be used as an intermediary between global circulation models and ice sheet models. We expect that PICO will be useful for providing ocean forcing to ice sheet models with the standardized input from climate model intercomparison projects like CMIP5 and CMIP6 (Taylor et al., 2012; Meehl et al., 2014; Eyring et al., 2016). Since PICO can deal with evolving ice shelf geometries in a computationally efficient way, it is in particular suitable for modeling the ice sheet evolution on paleo-climate timescales as well as for future projections.

PICO is implemented as a module in the open-source Parallel Ice Sheet Model (PISM). The source code is fully accessible and documented as we want to encourage improvements and implementation in other ice sheet models. This includes the adaption to other ice sheets than present-day Antarctica.

## 6 Code availability

The PICO code is part of the PISM-PIK development branch and openly available<sup>4</sup>. A merge into the general PISM stable version ~~08-1.0~~ 1.0 is underway.

## Appendix A: Derivation of the analytic solutions

Here, we derive the analytic solutions of the equations system describing the overturning circulation (see Sect. 2.1) and the melting at the ice-ocean interface (see Sect. 2.2).

For box  $B_k$  with  $k > 1$  we solve progressively for melt rate  $m_k$ , temperature  $T_k$  and salinity  $S_k$  in box  $B_k$ , dependent on the local pressure  $p_k$ , the area of box adjacent to the ice shelf base  $A_k$  and the temperature  $T_{k-1}$  and salinity  $S_{k-1}$  of the upstream box  $B_{k-1}$ . For box  $B_1$ , we additionally solve for the overturning  $q$  as explained below. These derivations advance the ideas presented in the appendix of OH10. Assuming steady state conditions, the balance equations Eqs. 1 and 2 for box  $B_k$  from

---

<sup>4</sup><https://github.com/pism/pism>

Sect. 2.1 are

$$\begin{aligned}
 0 &= q(T_{k-1} - T_k) + A_k \gamma_T (T_{bk} - T_k) + A_k m_k (T_{bk} - T_k) \\
 0 &= q(S_{k-1} - S_k) + A_k \gamma_S (S_{bk} - S_k) + A_k m_k (S_{bk} - S_k)
 \end{aligned}
 \tag{A1}$$

The heat fluxes balance at the boundary layer interface, *i.e.*, the heat flux across the boundary layer due to turbulent mixing

- 5  $Q_T = \rho_w c_p \gamma_T (T_{bk} - T_k)$  equals the heat flux due to melting or freezing  $Q_{Tb} = -\rho_i L m_k$ , omitting the heat flux into the ice. This yields

$$\gamma_T (T_{bk} - T_k) = -\nu \lambda m_k,
 \tag{A2}$$

where  $\nu = \rho_i / \rho_w \sim 0.89$ ,  $\lambda = L / c_p \sim 84^\circ\text{C}$ . Regarding the salt flux balance in the boundary layer, with  $Q_S = \rho_w \gamma_S (S_{bk} - S_k)$  at the lower interface of the boundary layer and “virtual” salt flux due to meltwater input  $Q_{Sb} = -\rho_i S_{bk} m_k$ , we obtain

$$10 \quad \gamma_S (S_{bk} - S_k) = -\nu S_{bk} m_k.
 \tag{A3}$$

Inserting Eqs. A2 and A3 into Eqs. A1 yields

$$\begin{aligned}
 0 &= q(T_{k-1} - T_k) - A_k m_k \nu \lambda + A_k m_k (T_{bk} - T_k) \\
 0 &= q(S_{k-1} - S_k) - A_k m_k \nu S_{bk} + A_k m_k (S_{bk} - S_k).
 \end{aligned}$$

- Comparing  $(T_{bk} - T_K) \ll \nu \lambda \approx 75^\circ\text{C}$ , allows us to neglect the last term in the temperature equation. Considering the last  
 15 two terms of the salinity equation, we find that  $S_k > (1 - \nu) S_{bk} \approx 0.1 S_{bk}$ , allowing us to neglect the terms containing  $S_{bk}$ , which simplifies the equations to

$$\begin{aligned}
 0 &= q(T_{k-1} - T_k) - A_k \nu \lambda m_k \\
 0 &= q(S_{k-1} - S_k) - A_k m_k S_k.
 \end{aligned}
 \tag{A4}$$

- We use a simplified version of the melt law described by McPhee (1992) and detailed in Sect. 2.2, which makes use of Eqn. 6  
 20 and Eqn. 5 in which the salinity in the boundary layer  $S_{bk}$  is replaced by salinity of the ambient ocean water.

$$m_{\underline{1}k} = -\frac{\gamma_T^*}{\nu \lambda} (a S_k + b - c p_k - T_k).
 \tag{A5}$$

Holland and Jenkins (1999) suggest that this simplification requires  $\gamma_T^*$  to be a factor of 1.35 to 1.6 smaller than  $\gamma_T$  in the 3-  
 25 equation formulation for the constant values of  $\gamma_T$  ranging from  $3 \times 10^{-5} \text{ m s}^{-1}$  to  $5 \times 10^{-5} \text{ m s}^{-1}$  used in OH10. This implies that  $\gamma_T^*$  ranges from  $2.2 \times 10^{-5} \text{ m s}^{-1}$  to  $3.2 \times 10^{-5} \text{ m s}^{-1}$ , which is consistent with the parameter range we derive in Sect. 3.1.

We apply this assumption in the computation of melt rates. For the solution of the transport equations A1, it is essential to take the salinity of the boundary layer  $S_{bk}$  into account, since otherwise the salinity transport equation would reduce to  $S_k = S_{k-1}$  and the overturning circulation, which is predominantly haline-driven, would be reduced. Inserting the simplified melt law in

Eqs. A4 yields

$$0 = q(T_{k-1} - T_k) + A_k \frac{\gamma_T^*}{\nu\lambda} (aS_k + b - cp_k - T_k) \nu\lambda$$

$$0 = q(S_{k-1} - S_k) + A_k \frac{\gamma_T^*}{\nu\lambda} (aS_k + b - cp_k - T_k) S_1$$

Replacing  $x = T_{k-1} - T_k$ ,  $y = S_{k-1} - S_k$ ,  $T^* = aS_{k-1} + b - cp_k - T_{k-1}$ ,  $g_1 = A_k \gamma_T^*$  and  $g_2 = \frac{g_1}{\nu\lambda}$ , we obtain

$$5 \quad 0 = qx + g_1(T^* + x - ay) \tag{A6}$$

$$0 = qy + g_2(S_{k-1} - y)(T^* + x - ay) \tag{A7}$$

We simplify the previous equations as follows. Rewriting Eq. A6

$$(T^* + x - ay) = \frac{-qx}{g_1}$$

and inserting it into Eq. A7, we obtain

$$10 \quad 0 = qy + g_2(S_{k-1} - y) \left( -\frac{qx}{g_1} \right) = qy - qx \frac{S_{k-1} - y}{\nu\lambda}$$

$$\iff 0 = \nu\lambda y - S_{k-1}x + xy$$

$$\iff 0 = (\nu\lambda + x)y - S_{k-1}x$$

$$\Rightarrow y = \frac{S_{k-1}x}{\nu\lambda + x}.$$

Note that we can divide the first line by  $q$  since, by the model assumptions,  $q > 0$ . Because  $x = T_{k-1} - T_k \ll \nu\lambda \approx 75^\circ\text{C}$ ,  
 15 we may approximate

$$y \approx \frac{S_{k-1}x}{\nu\lambda}. \tag{A8}$$

Using this approximation, we may proceed to solve the system of equations. Since we also need to solve for the overturning  $q$  in box  $B_1$ , which is adjacent to the grounding line, a slightly different approach is needed than for the other boxes, as discussed in the next section.

## 20 **Solution for box $B_1$**

The overturning flux  $q$  is parameterized as

$$q = C\rho_* (\beta(S_0 - S_1) - \alpha(T_0 - T_1)), \tag{A9}$$

in the model, see Sect. 2.1. Substituting this equation into Eqs. A6 and A7, we obtain

$$0 = \alpha x^2 - \beta xy - \frac{g_1}{C\rho_*} (T^* + x - ay) \tag{A10}$$

$$25 \quad 0 = -\beta y^2 + \alpha xy - \frac{g_2}{C\rho_*} (S_0 - y)(T^* + x - ay). \tag{A11}$$

Inserting the approximation for  $y$  from Eqn. A8 into the Eqn. A10, we obtain a quadratic equation for  $x$ ,

$$(\beta s - \alpha)x^2 + \frac{g_1}{C\rho_*}(T^* + x(1 - as)) = 0$$

with  $s = S_0/\nu\lambda$ . Since  $as = -0.057 \times S_0/74.76 = -0.000762 \times S_0 \ll 1$ , we can omit the last part of the last term,

$$(\beta s - \alpha)x^2 + \frac{g_1}{C\rho_*}(T^* + x) = 0.$$

5 Rearranging (assuming that  $\beta s - \alpha > 0$ , which we demonstrate below), we obtain

$$x^2 + \frac{g_1}{C\rho_*(\beta s - \alpha)}x + \frac{g_1 T^*}{C\rho_*(\beta s - \alpha)} = 0,$$

and hence we obtain the solution

$$x = -\frac{g_1}{2C\rho_*(\beta s - \alpha)} \pm \sqrt{\left(\frac{g_1}{2C\rho_*(\beta s - \alpha)}\right)^2 - \frac{g_1 T^*}{C\rho_*(\beta s - \alpha)}}. \quad (\text{A12})$$

The temperature in the box  $B_1$  near the grounding line is supposed to be smaller than in the ocean box  $B_0$ , since, in general,  
 10 melting will occur in box  $B_1$  and hence  $T_1 < T_0$ , or equivalently  $x = T_0 - T_1 > 0$ . Furthermore, we know that  $g_1/(C\rho_*) = A_1\gamma_T^*/(C\rho_*)$  is positive, as all factors are positive. Since  $\alpha = 7.5 \times 10^{-5}$ ,  $\beta = 7.7 \times 10^{-4}$  and  $s = S_0/(\nu\lambda) = S_0/74.76 \geq 0.4$ , it follows that  $\beta s > \alpha$ . This means that the first summand of Eqs. A12 is negative and the second (negative) solution can be excluded. From here, we use  $T_1 = T_0 + x$  and  $y = xS_0/(\nu\lambda)$  to solve for  $T_1$ ,  $S_1$ ,  $m_1$  and  $q$ .

### Solution for box $B_k$ , $k > 1$

15 Now, we give the solution for the other boxes  $B_k$  with  $k > 1$ . By inserting the approximation for  $y$  in Eqs A8 into Eq. A6, we can solve for  $x$  as

$$\begin{aligned} 0 &= qx + g_1 \left( T^* + x - a \frac{S_{k-1}x}{\nu\lambda} \right) \\ \iff 0 &= qx + g_1 T^* + g_1 x - g_2 a S_{k-1} x \\ \iff -g_1 T^* &= x(q + g_1 - g_2 S_{k-1} a) \\ 20 \iff x &= \frac{-g_1 T^*}{q + g_1 - g_2 a S_{k-1}}. \end{aligned} \quad (\text{A13})$$

The denominator is positive, as all terms are positive, and the sign of the numerator depends on  $T^*$ . The equation can now be solved for  $T_k$ , and then Eqn. A8 for  $S_k$  and Eqn. 13 for  $m_k$ .

### Appendix B: Motivation for geometric rule

Here, we want to motivate the rule that determines the extent of the boxes under each ice shelf. The rule aims at equal  
 25 areas for all boxes. Assuming a half-circle with radius  $r = 1$ , we want to split it into a fixed number  $n$  of equal-area rings.

Generalized to the individual shapes of ice-shelf basins, we will define the “radius” of an ice shelf as  $r = 1 - d_{\text{GL}}/(d_{\text{GL}} + d_{\text{IF}})$ . We define  $r_1 = 1$  the outer (grounding-line ward) radius of the half-circle ring covering an area  $A_1$  and corresponding to box  $B_1$  adjacent to the grounding line,  $r_2$  as the outer radius of second outer-most half-ring, etc. The box  $B_k$  is then given by all shelf cells with horizontal coordinates  $(x, y)$  such that  $r_{k+1} \leq r(x, y) \leq r_k$  where  $r_{n+1} = 0$  is the center point of the circle. We can use these to determine the areas  $A_n = 0.5\pi r_n^2$ ,  $A_{n-1} = 0.5\pi(r_{n-1}^2 - r_n^2)$ ,  $\dots$ ,  $A_{n-k} = 0.5\pi(r_{n-k}^2 - r_{n-k+1}^2)$ . If we require that  $A_1 = A_2 = \dots = A_n$ , then, solving progressively,  $r_{n-k} = \sqrt{k+1} r_n$ . By our assumption is  $r_1 = 1$ , hence  $1 = r_{n-(n-1)} = \sqrt{n} r_n$ . This implies that  $r_n = 1/\sqrt{n}$  and thus  $r_{n-k} = \sqrt{\frac{k+1}{n}}$ . Hence, the box  $B_k$  for  $k = 1, \dots, n$  is defined as  $1 - \sqrt{(n-k+1)/n} \leq d_{\text{GL}}/(d_{\text{GL}} + d_{\text{IF}}) \leq 1 - \sqrt{(n-k)/n}$ .

*Acknowledgements.* PISM development is supported by the NASA Modeling, Analysis, and Prediction program grant number NNX13AM16G and the NASA Cryospheric Sciences program grant number NNX16AQ40G and by NSF Polar Programs grants PLR-1603799 and PLR-1644277. T. A. was supported by DFG priority program SPP 1158, project numbers LE1448/6-1 and LE1448/7-1. M. M. was supported by the AXA Research Fund. [R. R. was supported by the German Academic National Foundation and the Evangelisches Studienwerk Villigst.](#) The project is further supported by the German Climate Modeling Initiative (PalMod) and the Leibniz project DominoES. X. A. D. was supported by the US Department of Energy, Office of Science, Office of Biological and Environmental Research under award no. DE-SC0013038. The authors gratefully acknowledge the European Regional Development Fund (ERDF), the German Federal Ministry of Education and Research and the Land Brandenburg for supporting this project by providing resources on the high performance computer system at the Potsdam Institute for Climate Impact Research.

## References

- Asay-Davis, X. S., Cornford, S. L., Durand, G., Galton-Fenzi, B. K., Gladstone, R. M., Gudmundsson, G. H., Hattermann, T., Holland, D. M., Holland, D., Holland, P. R., Martin, D. F., Mathiot, P., Pattyn, F., and Seroussi, H.: Experimental design for three interrelated marine ice sheet and ocean model intercomparison projects: MISMIP v. 3 (MISMIP+), ISOMIP v. 2 (ISOMIP+) and MISOMIP v. 1 (MISOMIP1), *Geoscientific Model Development*, 9, 2471–2497, doi:10.5194/gmd-9-2471-2016, 2016.
- 5 Beckmann, A. and Goosse, H.: A parameterization of ice shelf–ocean interaction for climate models, *Ocean Modelling*, 5, 157 – 170, doi:http://dx.doi.org/10.1016/S1463-5003(02)00019-7, 2003.
- Bueler, E. and Brown, J.: Shallow shelf approximation as a “sliding law” in a thermomechanically coupled ice sheet model, *Journal of Geophysical Research*, 114, doi:10.1029/2008JF001179, 2009.
- 10 Carroll, D., Sutherland, D. A., Shroyer, E. L., Nash, J. D., Catania, G. A., and Stearns, L. A.: Modeling Turbulent Subglacial Meltwater Plumes: Implications for Fjord-Scale Buoyancy-Driven Circulation, *Journal of Physical Oceanography*, 45, 2169–2185, doi:10.1175/JPO-D-15-0033.1, 2015.
- De Rydt, J. and Gudmundsson, G. H.: Coupled ice shelf-ocean modeling and complex grounding line retreat from a seabed ridge, *Journal of Geophysical Research: Earth Surface*, 121, 865–880, doi:10.1002/2015JF003791, 2015JF003791, 2016.
- 15 Depoorter, M. a., Bamber, J. L., Griggs, J. a., Lenaerts, J. T. M., Ligtenberg, S. R. M., van den Broeke, M. R., and Moholdt, G.: Calving fluxes and basal melt rates of Antarctic ice shelves., *Nature*, 502, 89–92, doi:10.1038/nature12567, 2013.
- Dupont, T. K. and Alley, R. B.: Assessment of the importance of ice-shelf buttressing to ice-sheet flow, *Geophysical Research Letters*, 32, doi:10.1029/2004GL022024, 104503, 2005.
- Eyring, V., Bony, S., Meehl, G. A., Senior, C. A., Stevens, B., Stouffer, R. J., and Taylor, K. E.: Overview of the Coupled Model Intercomparison Project Phase 6 (CMIP6) experimental design and organization, *Geoscientific Model Development*, 9, 1937–1958, doi:10.5194/gmd-9-1937-2016, 2016.
- 20 Favier, L., Durand, G., Cornford, S. L., Gudmundsson, G. H., Gagliardini, O., Gillet-Chaulet, F., Zwinger, T., Payne, A. J., and Le Brocq, a. M.: Retreat of Pine Island Glacier controlled by marine ice-sheet instability, *Nature Climate Change*, 5, 117–121, doi:10.1038/nclimate2094, 2014.
- 25 Feldmann, J., Albrecht, T., Khroulev, C., Pattyn, F., and Levermann, A.: Resolution-dependent performance of grounding line motion in a shallow model compared with a full-Stokes model according to the MISMIP3d intercomparison, *Journal of Glaciology*, 60, 353–360, doi:doi:10.3189/2014JoG13J093, 2014.
- Fretwell, P., Pritchard, H. D., Vaughan, D. G., Bamber, J. L., Barrand, N. E., Bell, R., Bianchi, C., Bingham, R. G., Blankenship, D. D., Casassa, G., Catania, G., Callens, D., Conway, H., Cook, A. J., Corr, H. F. J., Damaske, D., Damm, V., Ferraccioli, F., Forsberg, R., Fujita, 30 S., Gim, Y., Gogineni, P., Griggs, J. A., Hindmarsh, R. C. A., Holmlund, P., Holt, J. W., Jacobel, R. W., Jenkins, A., Jokat, W., Jordan, T., King, E. C., Kohler, J., Krabill, W., Riger-Kusk, M., Langley, K. A., Leitchenkov, G., Leuschen, C., Luyendyk, B. P., Matsuoka, K., Mouginot, J., Nitsche, F. O., Nogi, Y., Nost, O. A., Popov, S. V., Rignot, E., Rippin, D. M., Rivera, A., Roberts, J., Ross, N., Siegert, M. J., Smith, A. M., Steinhage, D., Studinger, M., Sun, B., Tinto, B. K., Welch, B. C., Wilson, D., Young, D. A., Xiangbin, C., and Zirizzotti, A.: Bedmap2: improved ice bed, surface and thickness datasets for Antarctica, *The Cryosphere*, 7, 375–393, doi:10.5194/tc-7-375-2013, 35 2013.

- Goldberg, D. N., Little, C. M., Sergienko, O. V., Gnanadesikan, A., Hallberg, R., and Oppenheimer, M.: Investigation of land ice-ocean interaction with a fully coupled ice-ocean model: 1. Model description and behavior, *Journal of Geophysical Research: Earth Surface*, 117, doi:10.1029/2011JF002246, f02037, 2012.
- Greenbaum, J. S., Blankenship, D. D., Young, D. a., Richter, T. G., Roberts, J. L., Aitken, a. R. a., Legresy, B., Schroeder, D. M., Warner, R. C., van Ommen, T. D., and Siegert, M. J.: Ocean access to a cavity beneath Totten Glacier in East Antarctica, *Nature Geoscience*, 8, doi:10.1038/NNGEO2388, 2015.
- Gudmundsson, G. H., Krug, J., Durand, G., Favier, L., and Gagliardini, O.: The stability of grounding lines on retrograde slopes, *The Cryosphere*, 6, 1497–1505, doi:10.5194/tc-6-1497-2012, 2012.
- Hellmer, H. and Olbers, D.: A two-dimensional model for the thermohaline circulation under an ice shelf, *Antarctic Science*, 1, 325–336, doi:10.1017/S0954102089000490, 1989.
- Hellmer, H. H., Kauker, F., Timmermann, R., and Hattermann, T.: The fate of the southern Weddell Sea continental shelf in a warming climate, *Journal of Climate*, 0, doi:10.1175/JCLI-D-16-0420.1, 2017.
- Holland, D. M. and Jenkins, A.: Modeling Thermodynamic Ice–Ocean Interactions at the Base of an Ice Shelf, *Journal of Physical Oceanography*, 29, 1787–1800, doi:10.1175/1520-0485(1999)029<1787:MTIOIA>2.0.CO;2, 1999.
- Holland, D. M., Thomas, R. H., de Young, B., Ribergaard, M. H., and Lyberth, B.: Acceleration of Jakobshavn Isbræt triggered by warm subsurface ocean waters, *Nature Geoscience*, 1, 659–664, doi:10.1038/ngeo316, 2008a.
- Holland, P. R., Feltham, D. L., and Jenkins, A.: Ice Shelf Water plume flow beneath Filchner-Ronne Ice Shelf, Antarctica, *Journal of Geophysical Research: Oceans*, 112, doi:10.1029/2006JC003915, c05044, 2007.
- Holland, P. R., Jenkins, A., and Holland, D. M.: The Response of Ice Shelf Basal Melting to Variations in Ocean Temperature, *Journal of Climate*, 21, 2558–2572, doi:10.1175/2007JCLI1909.1, 2008b.
- Hutter, K.: *Theoretical glaciology: material science of ice and the mechanics of glaciers and ice sheets*, vol. 1, Springer, 1983.
- Jacobs, S., Helmer, H., Doake, C. S. M., Jenkins, A., and Frolich, R. M.: Melting of ice shelves and the mass balance of Antarctica, *Journal of Glaciology*, 38, 375–387, doi:10.3198/1992JoG38-130-375-387, 1992.
- Jacobs, S. S., Jenkins, A., Giulivi, C. F., and Dutrieux, P.: Stronger ocean circulation and increased melting under Pine Island Glacier ice shelf, *Nature Geoscience*, 4, 519–523, doi:10.1038/ngeo1188, 2011.
- Jenkins, A.: A one-dimensional model of ice shelf-ocean interaction, *Journal of Geophysical Research: Oceans*, 96, 20 671–20 677, doi:10.1029/91JC01842, 1991.
- Jenkins, A.: Convection-Driven Melting near the Grounding Lines of Ice Shelves and Tidewater Glaciers, *Journal of Physical Oceanography*, 41, 2279–2294, doi:10.1175/JPO-D-11-03.1, 2011.
- Jenkins, A., Hellmer, H. H., and Holland, D. M.: The Role of Meltwater Advection in the Formulation of Conservative Boundary Conditions at an Ice–Ocean Interface, *Journal of Physical Oceanography*, 31, 285–296, doi:10.1175/1520-0485(2001)031<0285:TROMAI>2.0.CO;2, 2001.
- Joughin, I., Alley, R. B., and Holland, D. M.: Ice-Sheet Response to Oceanic Forcing, *Science*, 338, 1172–1176, doi:10.1126/science.1226481, 2012.
- Joughin, I., Smith, B. E., and Medley, B.: Marine Ice Sheet Collapse Potentially Under Way for the Thwaites Glacier Basin, West Antarctica, *Science*, 344, 735–738, doi:10.1126/science.1249055, 2014.
- Lewis, E. L. and Perkin, R. G.: Ice pumps and their rates, *Journal of Geophysical Research: Oceans*, 91, 11 756–11 762, doi:10.1029/JC091iC10p11756, 1986.

- Little, C. M., Goldberg, D., Gnanadesikan, A., and Oppenheimer, M.: On the coupled response to ice-shelf basal melting, *Journal of Glaciology*, 58, 203–215, doi:10.3189/2012JoG11J037, 2012.
- Liu, Y., Moore, J. C., Cheng, X., Gladstone, R. M., Bassis, J. N., Liu, H., Wen, J., and Hui, F.: Ocean-driven thinning enhances iceberg calving and retreat of Antarctic ice shelves, *Proceedings of the National Academy of Sciences*, 112, 3263–3268, doi:10.1073/pnas.1415137112, 5 2015.
- MacGregor, J. A., Catania, G. A., Markowski, M. S., and Andrews, A. G.: Widespread rifting and retreat of ice-shelf margins in the eastern Amundsen Sea Embayment between 1972 and 2011, *Journal of Glaciology*, 58, 458–466, doi:10.3189/2012JoG11J262, 2012.
- Martin, M. A., Winkelmann, R., Haseloff, M., Albrecht, T., Bueler, E., Khroulev, C., and Levermann, A.: The Potsdam Parallel Ice Sheet Model (PISM-PIK) – Part 2: Dynamic equilibrium simulation of the Antarctic ice sheet, *The Cryosphere*, 5, 727–740, doi:10.5194/tc-5-10 727-2011, 2011.
- McDougall, T. J. and Barker, P. M.: Getting started with TEOS-10 and the Gibbs Seawater (GSW) Oceanographic Toolbox, May, SCOR/IAPSO WG1207, [http://www.teos-10.org/pubs/Getting\\_Started.pdf](http://www.teos-10.org/pubs/Getting_Started.pdf), 2011.
- McPhee, M. G.: Turbulent heat flux in the upper ocean under sea ice, *Journal of Geophysical Research: Oceans*, 97, 5365–5379, doi:10.1029/92JC00239, 1992.
- 15 McPhee, M. G.: Parameterization of mixing in the ocean boundary layer, *Journal of Marine Systems*, 21, 55 – 65, doi:[http://dx.doi.org/10.1016/S0924-7963\(99\)00005-6](http://dx.doi.org/10.1016/S0924-7963(99)00005-6), 1999.
- Meehl, G. A., Moss, R., Taylor, K. E., Eyring, V., Stouffer, R. J., Bony, S., and Stevens, B.: Climate Model Intercomparisons: Preparing for the Next Phase, *Eos, Transactions American Geophysical Union*, 95, 77–78, doi:10.1002/2014EO090001, 2014.
- Mercer, J. H.: West Antarctic ice sheet and CO<sub>2</sub> greenhouse effect- A threat of disaster, *Nature*, 271, 321–325, 1978.
- 20 Moholdt, G., Padman, L., and Fricker, H. A.: Basal mass budget of Ross and Filchner-Ronne ice shelves, Antarctica, derived from Lagrangian analysis of ICESat altimetry, *Journal of Geophysical Research: Earth Surface*, 119, 2361–2380, doi:10.1002/2014JF003171, 2014JF003171, 2014.
- Moholdt, G., Padman, L., and Fricker, H. A.: Elevation change and mass budget of Ross and Filchner-Ronne ice shelves, Antarctica, doi:10.21334/npolar.2016.cae21585, <https://doi.org/10.21334/npolar.2016.cae21585>, 2016.
- 25 Morland, L. W.: *Unconfined Ice-Shelf Flow*, pp. 99–116, Springer Netherlands, Dordrecht, doi:10.1007/978-94-009-3745-1\_6, 1987.
- Mouginot, J., Rignot, E., and Scheuchl, B.: Sustained increase in ice discharge from the Amundsen Sea Embayment, West Antarctica, from 1973 to 2013, *Geophysical Research Letters*, 41, 1576–1584, doi:10.1002/2013GL059069, 2014.
- Nowicki, S. M. J., Payne, A., Larour, E., Seroussi, H., Goelzer, H., Lipscomb, W., Gregory, J., Abe-Ouchi, A., and Shepherd, A.: Ice Sheet Model Intercomparison Project (ISMIP6) contribution to CMIP6, *Geoscientific Model Development*, 9, 4521–4545, doi:10.5194/gmd-9-30 4521-2016, 2016.
- Olbers, D. and Hellmer, H.: A box model of circulation and melting in ice shelf caverns, *Ocean Dynamics*, 60, 141–153, doi:10.1007/s10236-009-0252-z, 2010.
- Paolo, F. S., Fricker, H. A., and Padman, L.: Volume loss from Antarctic ice shelves is accelerating, *Science*, 348, 327–332, doi:10.1126/science.aaa0940, 2015.
- 35 Pattyn, F., Perichon, L., Durand, G., Favier, L., Gagliardini, O., Hindmarsh, R. C., Zwinger, T., Albrecht, T., Cornford, S., Docquier, D., Fürst, J. J., Goldberg, D., Gudmundsson, G. H., Humbert, A., Hütten, M., Huybrechts, P., Jouvét, G., Kleiner, T., Larour, E., Martin, D., Morlighem, M., Payne, A. J., Pollard, D., Rückamp, M., Rybak, O., Seroussi, H., Thoma, M., and Wilkens, N.: Grounding-line

- migration in plan-view marine ice-sheet models: results of the ice2sea MISMIP3d intercomparison, *Journal of Glaciology*, 59, 410–422, doi:doi:10.3189/2013JoG12J129, 2013.
- Payne, A. J., Holland, P. R., Shepherd, A. P., Rutt, I. C., Jenkins, A., and Joughin, I.: Numerical modeling of ocean-ice interactions under Pine Island Bay's ice shelf, *Journal of Geophysical Research: Oceans*, 112, doi:10.1029/2006JC003733, c10019, 2007.
- 5 Pollard, D. and DeConto, R. M.: Description of a hybrid ice sheet-shelf model, and application to Antarctica, *Geoscientific Model Development*, 5, 1273–1295, doi:10.5194/gmd-5-1273-2012, 2012.
- Pritchard, H. D., Ligtenberg, S. R. M., Fricker, H. A., Vaughan, D. G., van den Broeke, M. R., and Padman, L.: Antarctic ice-sheet loss driven by basal melting of ice shelves, *Nature*, 484, 502–505, doi:10.1038/nature10968, 2012.
- Rignot, E., Jacobs, S., Mouginot, J., and Scheuchl, B.: Ice-shelf melting around Antarctica., *Science*, 341, 266–270, doi:10.1126/science.1235798, 2013.
- 10 Schmidtko, S., Heywood, K. J., Thompson, A. F., and Aoki, S.: Multidecadal warming of Antarctic waters, *Science*, 346, 1227–1231, doi:10.1126/science.1256117, 2014.
- Schoof, C.: Marine ice-sheet dynamics. Part 1. The case of rapid sliding, *Journal of Fluid Mechanics*, 573, 27–55, 2007.
- Seroussi, H., Nakayama, Y., Larour, E., Menemenlis, D., Morlighem, M., Rignot, E., and Khazendar, A.: Continued retreat of Thwaites 15 Glacier, West Antarctica, controlled by bed topography and ocean circulation, *Geophysical Research Letters*, doi:10.1002/2017GL072910, 2017.
- Taylor, K. E., Stouffer, R. J., and Meehl, G. A.: An Overview of CMIP5 and the Experiment Design, *Bulletin of the American Meteorological Society*, 93, 485–498, doi:10.1175/BAMS-D-11-00094.1, 2012.
- Thoma, M., Jenkins, A., Holland, D., and Jacobs, S.: Modelling Circumpolar Deep Water intrusions on the Amundsen Sea continental shelf, 20 Antarctica, *Geophysical Research Letters*, 35, doi:10.1029/2008GL034939, 118602, 2008.
- Thoma, M., Determann, J., Grosfeld, K., Goeller, S., and Hellmer, H. H.: Future sea-level rise due to projected ocean warming beneath the Filchner Ronne Ice Shelf: A coupled model study, *Earth Planet. Sci. Lett.*, 431, 217–224, doi:10.1016/j.epsl.2015.09.013, 2015.
- Thomas, R. H.: Ice Shelves: a Review, *Journal of Glaciology*, 24, 273–286, doi:doi:10.3198/1979JoG24-90-273-286, 1979.
- Winkelmann, R., Martin, M. A., Haseloff, M., Albrecht, T., Bueler, E., Khroulev, C., and Levermann, A.: The Potsdam Parallel Ice Sheet 25 Model (PISM-PIK) – Part 1: Model description, *The Cryosphere*, 5, 715–726, doi:10.5194/tc-5-715-2011, 2011.
- Wouters, B., Martin-Espanol, A., Helm, V., Flament, T., van Wessem, J. M., Ligtenberg, S. R., van den Broeke, M. R., and Bamber, J. L.: Glacier mass loss. Dynamic thinning of glaciers on the Southern Antarctic Peninsula, *Science*, 348, 899–903, doi:10.1126/science.aaa5727, 2015.
- Zwally, H., Giovinetto, M., Beckley, M., and Saba, J.: *Antarctic and Greenland Drainage Systems*, 2012.

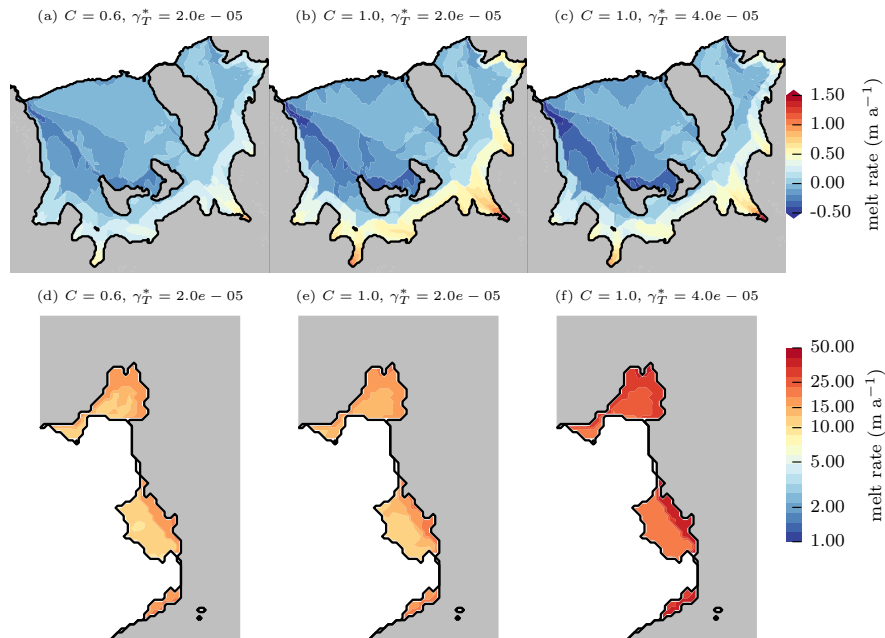


**Figure S.1.** Basal melt rates in the **Pine Island and Filchner-Ronne** (upper panels) and **Amundsen Sea** (lower panels) regions for different parameter combinations of the overturning strength  $C$  and the effective turbulent heat transfer coefficient  $\gamma_T^*$ . Grounded ice regions are shown in grey.

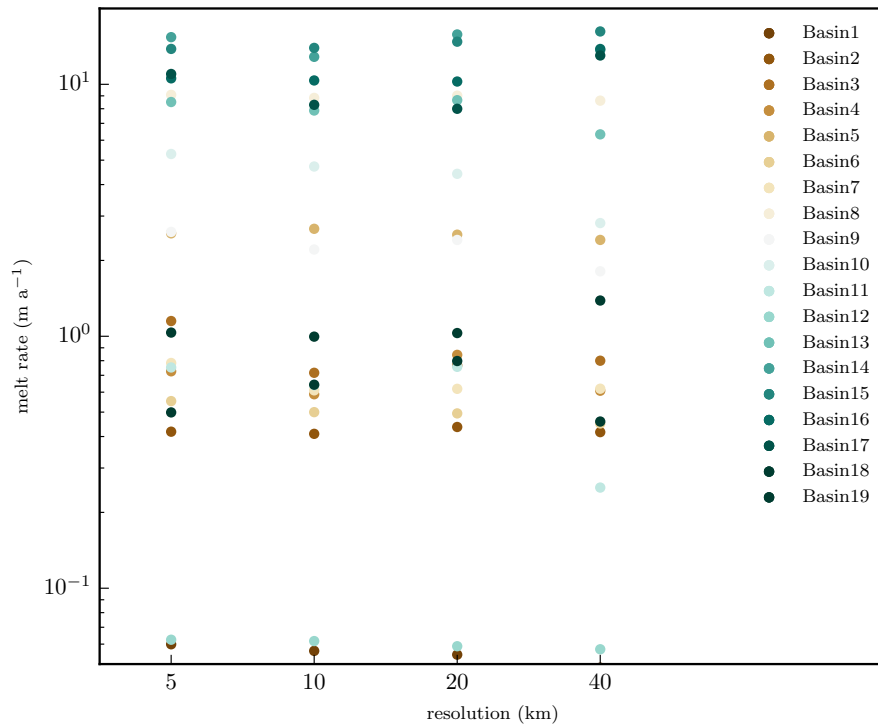


**Figure S.2.** Sensitivity of mean sub-shelf melt rates to the ice-sheet model resolution.

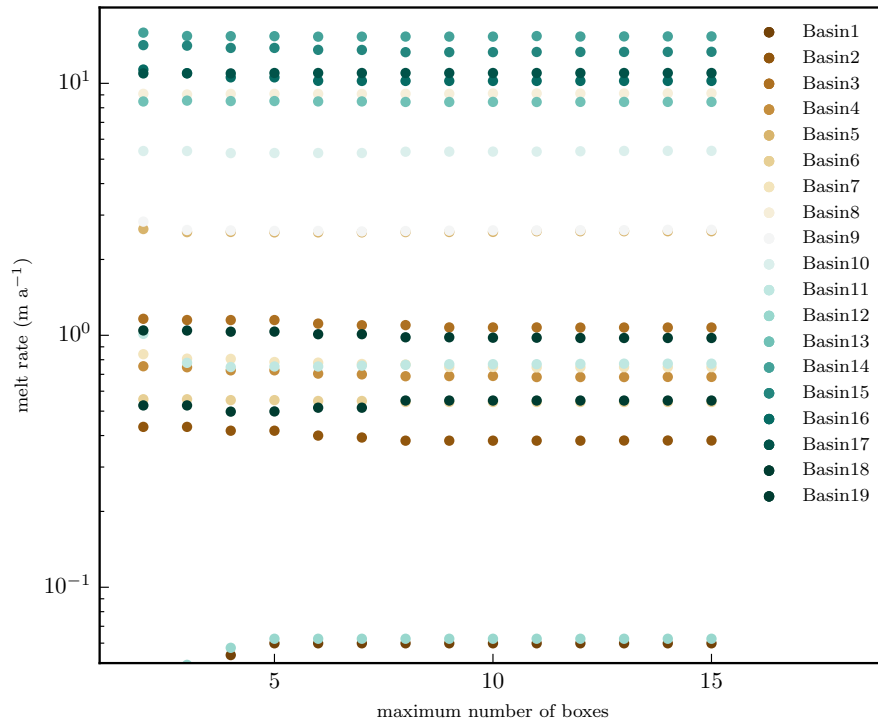


**Figure S.3.** Sensitivity of mean sub-shelf melt rates to the maximum number of boxes of PICO.

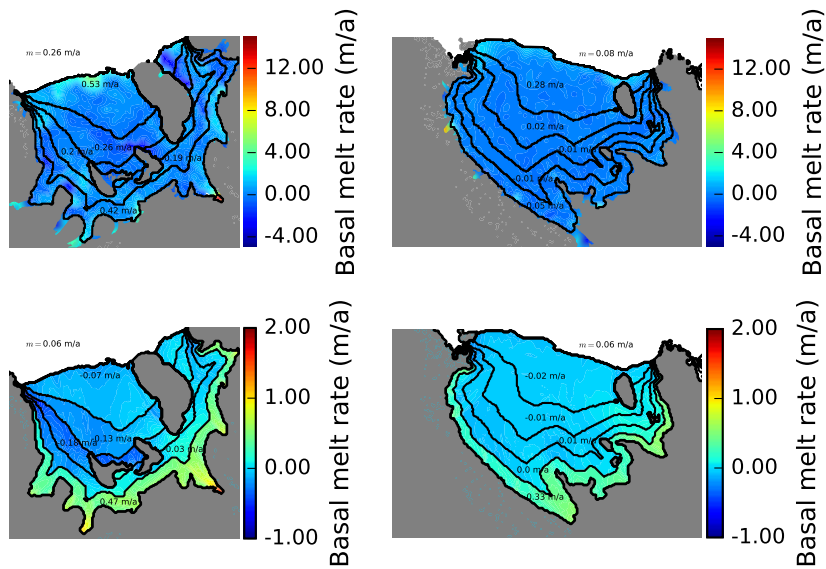


**Figure S.4.** Comparison of observed sub-shelf melt rates (upper row) from (Moholdt et al., 2016) with melt rates modelled by PICO (lower row) for Filchner-Ronne (left column) and Ross ice shelves (right column). Black contour lines indicate the PICO ocean boxes with annotations giving the box-wide average melt rates respectively. PICO tends to distribute melting, such that melt rate deviations are at a lower order of magnitude than in the observations. Nevertheless, box-wide averages show reasonable agreement.

**Table S.1.** Results from the reference simulation as displayed in Fig. 5.

| basin          | $m_\Sigma$         | $m_{\min}$       | $m_{\max}$       | $q$  | $m_\Sigma/q$ | $Q_{in}$           | $Q_{out}$          | $Q_m$              | $Q_\Delta$         | $Q_\Delta/Q_m$ | $b_1$ |
|----------------|--------------------|------------------|------------------|------|--------------|--------------------|--------------------|--------------------|--------------------|----------------|-------|
|                | Gt a <sup>-1</sup> | ma <sup>-1</sup> | ma <sup>-1</sup> | Sv   | %            | TJ s <sup>-1</sup> | TJ s <sup>-1</sup> | GJ s <sup>-1</sup> | GJ s <sup>-1</sup> | %              | m     |
| Wilkins(*)     | 320                | 0.26             | 19.80            | 0.32 | 3.06         | 361.30             | 357.90             | 3382.50            | 19.06              | 0.56           | 272   |
| Pine Island    | 61                 | 12.39            | 21.01            | 0.17 | 1.11         | 188.51             | 187.87             | 645.56             | 2.68               | 0.41           | 439   |
| Thwaites       | 53                 | 11.44            | 20.90            | 0.13 | 1.27         | 143.41             | 142.85             | 560.51             | 1.13               | 0.20           | 438   |
| Getz           | 112                | 2.48             | 10.78            | 0.23 | 1.48         | 260.10             | 258.90             | 1189.23            | 13.98              | 1.18           | 494   |
| Drygalski      | 1                  | 0.01             | 3.51             | 0.02 | 0.23         | 17.33              | 17.32              | 12.50              | -0.16              | -1.28          | 293   |
| Cook           | 7                  | 0.70             | 5.25             | 0.05 | 0.38         | 60.87              | 60.80              | 72.20              | -0.10              | -0.14          | 458   |
| Ninnis         | 4                  | 1.08             | 6.61             | 0.04 | 0.31         | 48.80              | 48.75              | 47.19              | -0.08              | -0.17          | 514   |
| Mertz          | 6                  | 0.38             | 4.60             | 0.04 | 0.45         | 43.27              | 43.21              | 60.18              | -0.14              | -0.23          | 309   |
| Totten         | 29                 | 5.93             | 14.33            | 0.13 | 0.70         | 144.10             | 143.79             | 309.81             | 1.06               | 0.34           | 677   |
| Shackleton     | 9                  | -0.21            | 2.70             | 0.07 | 0.40         | 77.62              | 77.52              | 96.93              | 0.48               | 0.50           | 270   |
| West           | 9                  | -0.08            | 5.26             | 0.07 | 0.38         | 78.82              | 78.73              | 93.34              | -0.17              | -0.18          | 428   |
| Amery          | 25                 | -1.22            | 5.93             | 0.16 | 0.49         | 175.86             | 175.58             | 269.19             | 11.89              | 4.42           | 674   |
| Baudouin       | 22                 | -0.25            | 2.73             | 0.12 | 0.59         | 128.92             | 128.68             | 234.16             | 7.03               | 3.00           | 325   |
| Fimbul         | 19                 | -0.25            | 2.97             | 0.10 | 0.57         | 115.85             | 115.64             | 204.02             | 5.79               | 2.84           | 303   |
| Riiser-Larsen  | 13                 | -0.22            | 1.83             | 0.09 | 0.46         | 94.92              | 94.78              | 136.36             | 3.84               | 2.82           | 273   |
| Brunt(**)      | 11                 | -0.16            | 2.30             | 0.08 | 0.40         | 93.81              | 93.69              | 117.21             | 3.31               | 2.83           | 250   |
| Filchner-Ronne | 21                 | -0.67            | 1.76             | 0.21 | 0.31         | 236.72             | 236.34             | 225.52             | 152.22             | 67.50          | 839   |
| Ross           | 25                 | -0.24            | 0.62             | 0.17 | 0.44         | 191.38             | 191.01             | 262.62             | 113.98             | 43.40          | 411   |
| Antarctica     | 1718               | -1.22            | 26.91            | 8.51 | 0.62         | 9473.42            | 9454.84            | 18183.19           | 403.63             | 2.22           | -     |

For each basin,  $m_\Sigma$  is the aggregated melt rate over the entire basin,  $q$  the overturning flux computed as average over box  $B_1$ ,  $m_\Sigma/q$  estimates the error in mass flux introduced by assuming constant overturning;  $Q_{in} = T_0 \times q \times c_p \times \rho_w$  is the heat flux from box  $B_0$  in box  $B_1$ ,  $Q_{out} = T_n \times q \times c_p \times \rho_w$  the flux from the last box  $B_n$  adjacent to the shelf front into the ocean,  $Q_m = Lm_\Sigma$  the heat flux due to melting of ice,  $Q_\Delta = Q_{in} - Q_{out} - Q_m$  the error in the heat balance.  $Q_\Delta/Q_m$  is the error in the heat balance relative to the heat flux for melting which results from the non-linearity of the temperature solution in box  $B_1$ . The average depth of this box is given by  $b_1$ . (\*) includes also Stange, Bach and George VI ice shelves and (\*\*) also Stancomb Ice Shelf.

**Video. S.1.** Based on an Antarctic equilibrium state at 8km resolution comparable to the state submitted to initMIP (Nowicki et al., 2016), PISM+PICO is forced with time-dependent ocean temperature input: Starting from equilibrium conditions, ocean temperatures increase linearly over 50 years until an ocean-wide warming of 1°C is reached. It is then held constant over the next 250 model years. The movie shows the temporal evolution of the ocean temperature input for the ice shelf adjacent to Pine Island Glacier as well as the Filchner-Ronne Ice Shelf (upper left panel). The ocean temperature increase enhances the average sub-shelf melting for both ice shelves (lower left panel, shown in logarithmic scale) with the spatial distribution of the melt rates for both ice shelves on the right hand side. During the simulation, the melt rates in both areas increase, especially in the first box (upper right panel shows Filchner-Ronne Ice Shelf and lower right panel the Amundsen region). Ice-shelf thinning reduces buttressing and causes the grounding lines to retreat (for example near Foundation Ice Stream in Filchner-Ronne Ice Shelf) with the ocean boxes adjusting accordingly.